Direct Evidence of Regimes I, II, and III in Linear Polyethylene Fractions As Revealed by Spherulite Growth Rates

J. P. Armistead*

Chemistry Division, Naval Research Laboratory, Washington D.C. 20375

John D. Hoffman

Department of Materials Science and Engineering, Johns Hopkins University, Baltimore, Maryland 21218

Received February 21, 2001; Revised Manuscript Received January 25, 2002

ABSTRACT: Isothermal spherulite growth rates were measured over a sufficient range of undercoolings, ΔT, for a narrow linear polyethylene fraction $M = 70\,300$ (70.3K), polydispersity 1.12, such that the fraction exhibited all three growth regimes as crystallized from the subcooled melt. The I−II transition occurred at $\Delta T_{I-II} = 15.8$ °C and the II−III transition at $\Delta T_{II-III} = 23.8$ °C. (Neither transition was fully abrupt.) The nucleation constants K_g and preexponential factors G_0 that described the absolute growth rates for each regime were determined, thus quantifying key parameters for all three regimes for a single specimen measured in the same apparatus. The K_g's for 70.3K conformed to the predicted relationship $K_{g(III)} \cong K_{g(I)} = 2K_{g(II)}$. Theoretical relationships for the preexponential factors were employed using the observed G_0's to investigate the nature of the transport of chain segments to the growth front. It was reconfirmed that this process was forced "near-ideal" reptation for an $M \cong 30$K fraction. For $M = 70.3$K, it was found that the reptational transport mechanism in regimes II and III was perturbed and thereby slowed beyond that attributable to "near-ideal" forced reptation; the additional retardation was taken to be the result of labile chain attachments on a surface some distance from the site where the dangling chain was being drawn onto the substrate. In another test, the expression S_k/a_o for the stem separation between primary surface nuclei in regime II was employed to calculate ΔT_{I-II} and ΔT_{II-III}. This was successful for both $M \cong 30$K (near-ideal reptation) and $M = 70.3$K (perturbed reptation). In this test, earlier estimates of quantities of importance to nucleation theory, such as C_0, n_{III}, and the substrate length L, were found to be either identical or only slightly modified. The treatment leads to satisfactory numerical estimates of the absolute substrate completion rate g and the nucleation rate i, and is consistent with the crystal morphology present in melt-crystallized PE, including the lenticular crystal → truncated lozenge transformation associated with the I → II regime transition. In general, this work provides significant additional support for the "three regime" concept in narrow PE fractions crystallized from the melt through a consideration of nucleation, regime, and reptation concepts.

Introduction

The purpose of this work is to extend application of surface nucleation theory in some detail to narrow melt-crystallized linear polyethylene (PE) fractions, particularly with respect to the temperature and molecular weight range where definite growth regime transitions occur. Flux-based nucleation theory combined with regime and reptation concepts allows prediction[1] of three growth rate regions denoted I, II, and III, in order of their appearance with descending isothermal crystallization temperature, T. Each regime has its own characteristic growth rate curve such that the existence of these regimes leads to a notable degree of structure in plots of the $\ln G + Q_D^*/RT$ against $1/T(\Delta T)$, where G is the spherulite growth rate and ΔT is the undercooling based on the appropriate T_m for the narrow fraction. When such plots (or plots of log G against T which in some instances can bring out regime effects) are properly analyzed they can be informative of the molecular mechanisms involved. Extensive earlier spherulite growth rate studies[1,2] have revealed the molecular weight range for linear PE where regimes I and II, and the transition between them, occur in distinct form for these chain-folded lamellar systems. Using $M_{nw} = (M_n \times M_w)^{1/2}$ as a measure of molecular mass, the I−II transition has been observed for 10 narrow PE fractions ranging from 15 300 (15.3K) to 90 600 (90.6K) g/mol. Thus, there are quantitative spherulite growth rate data for regimes I and II in this range. Fully characteristic I−II transitions with slope changes close to 2.0 do not occur above about $M_{nw} = 100$K, and interesting "quantized" crystallization effects associated with once, twice, and three-times adjacently folded structures intervene in the range $M_{nw} = 3.39$K to 11.0K; these two effects restrict the study of clear-cut regime phenomena in PE to the range of ∼15K to ∼90K.[1]

The situation for regime III and the II−III transition is less complete than that of I−II, regime III having been verified heretofore in terms of absolute growth rates for only one fraction, namely NBS SRM 1483 $M_n = 28.9$K, $M_w = 32.1$K, $M_{nw} = 30.5$K. (Henceforth this fraction is denoted $M_{nw} = 30.5$K or simply "30.5K", and will be taken to be a member of a group of narrow fractions of closely similar molecular weight under the general designation $M_{nw} \cong 30$K or $M \cong 30$K.) Support for the properties and existence of regime III for this fraction depend on growth rate estimates by Barham and others[3] obtained at 90 and 100 °C using a special technique involving micron-sized droplets. Following the precepts of nucleation theory, these data are plotted as $\ln G + Q_D^*/RT$ vs $1/T(\Delta T)$ in Figure 1 together with regime I and II spherulite growth rate results from earlier work[1,2] for a good PE fraction of the similar molecular weight $M_{nw} = 28.0$K. Here G is the spherulite growth rate in cm/s, $Q_D^* = 5736$ cal/mol, the activation energy of reptational diffusion, R is the gas constant,

10.1021/ma010313u CCC: $22.00
Published on Web 04/10/2002

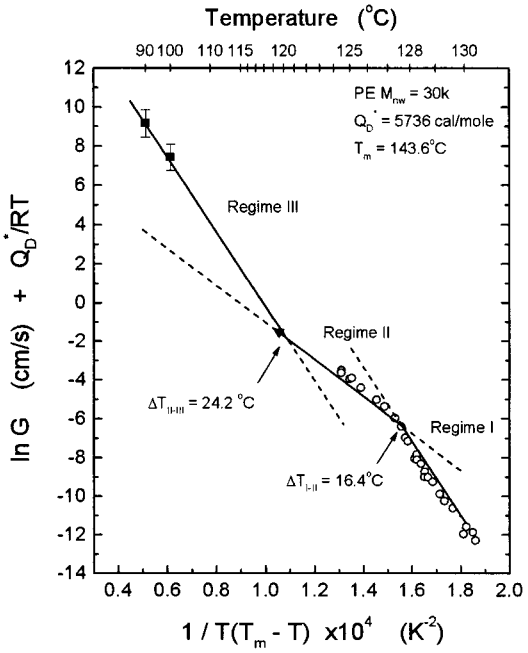

Figure 1. Plot of ln $G + Q_D^*/RT$ vs $1/T(\Delta T)$ showing three crystallization regimes in PE fractions $M_{nw} \cong 30$K: spherulite growth rates, ref 3 (■) and refs 1 and 2 (○); intersection temperature of regimes II and III from bulk crystallization rates, ref 4 (▼). Solid lines are based on theory with $K_{g(III)} = K_{g(I)} = 2K_{g(II)}$ (see text).

and ΔT is the undercooling $T_m - T$ where $T_m = 143.6$ °C for the $M_{nw} = 30.5$K fraction. In such a plot, theory calls for each regime to be represented by a straight line (except in the immediate vicinity of the transition), and the slopes of the regime I and III lines are to be close to the same and equal to twice the slope of the regime II line.[1] That the I−II transition occurs in $M \cong 30$K at $T_{I-II} \cong 127.2$ °C, $\Delta T_{I-II} = 16.4 \pm 0.5$ °C, is known from earlier work.[1,2] The construction in Figure 1 (intersection of heavy lines) marking the II−III transition temperature at $T_{II-III} \cong 119.4$ °C, $\Delta T_{II-III} \cong 24.2$ °C, closely corresponds to the T_{II-III} clearly seen experimentally in bulk crystallization rates as determined calorimetrically by Fatou et al.[4] It is evident that all three regimes are present. The composite picture of the regimes in Figure 1 (which is based on measurements by several groups of investigators as noted in the legend) is fully representative of the "three regime" effect as denoted by the characteristic slope changes of ~2.0 between them and will in due course be employed in a quantitative analysis for $M \cong 30$K. It remains to extend observation of regime III to a higher molecular weight narrow fraction to obtain a broader picture of crystallization behavior and to carry out further tests of the nucleation approach.

Pursuant to the above objective, we shall present spherulite growth rate data for a PE fraction $M_n = 66.4$K, $M_w = 74.4$K, polydispersity 1.12, $M_{nw} = 70.3$K (hereafter generally denoted $M_{nw} = 70.3$K) that clearly exhibits the three regimes during crystallization from the subcooled melt. (The $M_{nw} = 70.3$K specimen studied here is the same as fraction 9 of Table 2 in ref 1, the earlier work covering only regime I and the upper part of regime II.) The new results for $M_{nw} = 70.3$K represent an example where spherulite growth rate data bring out in terms of quantitative G values the properties of all three regimes for a narrow PE fraction measured in the same apparatus. Spherulite growth rates are emphasized here because the form of nucleation theory employed is cast in terms of nucleation constants, K_g, and the preexponential factors, G_0, characteristic of the absolute lineal growth rate in each regime—while approximate estimates of K_g and acceptable regime transition temperatures can be obtained from plots based on bulk growth rate data measured by calorimetric techniques, it is generally not possible to obtain useful G_0 values by such methods. For a given regime, i = I, II, or III, the relevant pair, $G_{0(i)}$, $K_{g(i)}$, describes the absolute growth rate G_i in that regime as a function of T and ΔT. A summary of the form of $G_{0(i)}$ and $K_{g(i)}$ and the ratios between them is given in the next section. It is these quantities that provide the basis for application and testing of the role of regime and reptation effects in nucleation theory.

One of the checks of the theory is afforded by comparing the experimental K_g's determined for $M_{nw} = 70.3$K for the three regimes with those found earlier for fractions in the vicinity of $M_{nw} \cong 30$K. These two fractions are in separate classes as regards the mechanism of chain transport to the growth front; for $M_{nw} \cong 30$K this mechanism is "near ideal" reptation and for $M_{nw} = 70.3$K it is the perceptibly slower "perturbed" reptation as revealed previously from regime I and II data on 10 narrow PE fractions.[1] ($M_{nw} \cong 30$K is typical of the set of 7 fractions $M_{nw} = 15.3$K to 38.6K, range $B-B'$ in ref 1, and $M_{nw} = 70.3$K is a typical member of the set of three fractions 53.5K to 90.6K, range $C-C'$ in ref 1). The $K_{g(i)}$'s, now including regime III as for i = III, will be shown for $M_{nw} = 70.3$K to conform in a satisfactory manner with theoretical expectation as regards their ratio to one another, their absolute magnitude, and the nearly invariant value of each $K_{g(i)}$ with change of molecular weight, irrespective of the difference in transport mechanism.

The perturbed reptation concept is revisited and confirmed for $M_{nw} = 70.3$K for regime II, and then extended here to the case of regime III. Transport effects are embodied in the preexponential factors $G_{0(II)}$ and $G_{0(III)}$, which permit at least approximate quantification of the perturbation effect in $M_{nw} = 70.3$K for each of the regimes. A molecular mechanism is proposed for the perturbation that is consistent with both the G_0 measurements and the reduced degree of crystallinity in the higher molecular weight 70.3K fraction.

Another test of the theory involves the function S_k/a_0, which gives the number of stems of width a_0 between primary nucleation acts in regime II. The quantity S_k/a_0 depends on the ratio $(2g/i)^{1/2}$ where g is the substrate completion rate and i is the surface nucleation rate. The function S_k/a_0 was previously successfully employed[1] to find the undercoolings ΔT_{I-II} and ΔT_{II-III} for the I−II and II−III transitions for $M_{nw} \cong 30$K (near-ideal reptation), and here it will be applied to $M_{nw} = 70.3$K (perturbed reptation) to estimate ΔT_{I-II} and ΔT_{II-III}. This is a test of the validity of the expressions derived for g and i, both expressions bearing a common factor representing the perturbation effect which should then cancel in the ratio g/i. It will be shown that this cancellation in fact occurs for $M_{nw} = 70.3$K and leads to accurate ΔT_{I-II} and ΔT_{II-III} values as well as acceptable results for the parameters n_{III} and n_L. The quantity n_{III} is related to the small separation between primary stems in regime III, and n_L is related to the substrate length L in regime I.

Other aspects of the treatment will be considered. One of these involves the sharpness of the regime transi-

tions. Previous studies of PE were not designed to deal with this question, but the present data for $M_{nw} = 70.3$K are of sufficient accuracy to show that neither the I−II nor II−III transition is completely abrupt. A discussion will be given concerning the deviations from sharp behavior, which are small and confined to the immediate vicinity of the regime transitions. Other topics discussed include reptation of "slack", the absence of distinct and ideal regime transitions in fractions for molecular weights in excess of 100K, and the relationship between spherulite morphology and regime transitions. The physical origin of the small and finite substrate length, L, that is required for a I−II transition to exist is revisited and related to the role of the lenticular crystal → truncated lozenge transformation at this regime transition. Also it will be shown that the treatment yields consistent numerical values for the surface nucleation rate i and substrate completion rate g. The claim that what we and others have termed "regime transitions" (and treated here and elsewhere[1] as being the result of nucleation effects) are actually artifacts caused by fractionation during crystallization will be countered. It will emerge that flux-based nucleation theory with regime and reptation effects considered provides a framework based on measurable parameters of stated physical origin that afford insights, now extended to include regime III at a higher molecular weight, into the mechanisms active in the crystallization of PE fractions $M_{nw} \sim 15$K to $M_{nw} \sim 90$K.

Theory

The summary expressions cited below arise from flux-based surface nucleation theory as applied to chain-folded lamellar systems consisting of flexible chains. On a coarse-grained basis the treatment considers forward and backward reactions for both deposition of the first (primary nucleating) stem as well as subsequent stems added in the ensuing substrate completion process, detailed balance applying in all cases. The formulas that follow are mostly from ref 1 and are based on the simple $\psi = 0$ or "low ψ" form of the theory which has no hypothetical abrupt upswing in the growth rate or lamellar thickness at low temperatures, i.e., no "δ catastrophe". In this format the surface free energy terms dominate the forward reactions, whether they be for the initial stem or subsequent adjacent stems, and the free energy of fusion terms dominate the corresponding backward reactions; i.e., the full free energy of fusion must be supplied to remove a stem. In PE, the dominant {110} growth front (substrate) is more or less perpendicular to the spherulite radius, each stem added having a similar orientation with respect to the radius. Growth in the radial direction is caused by successive addition of new layers of thickness b_0 generated by nucleation acts on the {110} substrate.

Unlike early traditional nucleation treatments based on the "saddle point" approach, the present theory gives expressions for the preexponential factors that among other items contain a transport term that includes the effect of chain length as it relates to reptation, a subject of interest here including the case of regime III. Reptation enters the picture because a partially attached chain dangling in the subcooled melt must be drawn by the force of crystallization (overcoming the resistance at entanglement points in that melt) on to the substrate in order to effect deposition of each successively added stem. Thus, one deals here in general with "forced" reptation.

The origin of chain folding in the treatment is clearly evident: when the high barrier to forming the first stem is overcome and that stem deposited on the surface, it now has an energetically favorable niche on either side each of which then invites the emergent chain to fill the niche forming a fold in the process. The act of chain folding tends to persist during the ensuing substrate completion process, again largely the result of the proximity of an emergent chain from the newly deposited stem to its energetically favorable adjacent niche. This is a probable rather than perfect process in PE and the folding is accordingly not totally regular, the degree of "tight" folding p_{tf} (p_{tf} = sum of adjacent re-entry and next-nearest re-entry, $p_{ar} + p_{arr}$) being 0.51−0.58 in regime III and rising to ∼0.82 in regime I for fractions near 40K; p_{ar} increases from ∼0.30 to ∼0.40 in regime III to ∼0.66 in regime I.[1] The "Gamblers Ruin" topological constraint that forbids an excess density at the fold surface defines the minimum degree of "tight" folding during substrate completion—the lowering of the degree of such folding with increasing ΔT, i.e., in going from regime I to regime III, is related to the increased angle of chain tilt.[1,5,6] Through the introduction of folds, reptation effects, and topological constraints, the chain connectivity of polymer molecules is inherent in the model at the outset. Moreover, the model will be seen to be consistent with the crystallography and crystal types present in the vicinity of the I−II transition in melt-crystallized PE.

The net surface nucleation rate i in number of stems cm^{-1} s^{-1} that determines the rate of deposition of the primary single-stem nucleus is

$$i = C_0 \frac{\kappa}{[(2/3)n]} \left(\frac{kT}{h}\right) \left[\frac{kT(\Delta h_f)(\Delta T)}{4 b_0 l_u \sigma^2 T_m}\right] \exp\left(\frac{-Q_D^*}{RT}\right) \times \exp\left(\frac{-[4] b_0 \sigma \sigma_e T_m}{\Delta h_f (\Delta T) kT}\right) \quad (1)$$

Here C_0 is the configurational path degeneracy (number of reaction paths to the activated state) and κ a numerical parameter that is inversely proportional to the monomeric friction coefficient ξ_0 associated with the reptation process in the melt; both of these constants are known for PE from previous work.[1] Further, k = Boltzmann constant, h = Planck constant, R = gas constant, Δh_f = heat of fusion, σ_e = fold surface free energy, σ = lateral surface free energy, l_u = length of $-CH_2-$ unit, b_0 = layer thickness on substrate, ΔT the undercooling $T_m - T$, where T_m is the equilibrium melting point for the molecular weight considered and T the isothermal crystallization temperature, Q_D^* the activation energy of the reptation process, and n the number of $-CH_2-$ units in the complete chain weighted with respect to the molecular weight distribution according to reptation concepts. In eq 1, the numerical quantity κ arises from the transport or retardation factor $\beta = (\kappa/n)(kT/h) \exp(-Q_D^*/RT)$ in the basic theory and is a convenient measure of the magnitude of the reptational transport process.[1] The factor $1/[(2/3)n]$ in the preexponential of i and other expressions in this work accounts for the time average number of $-CH_2-$ groups in a pendant chain in the act of being drawn on to the substrate by the force of crystallization; the factor of $^2/_3$ results from the fact that the chain under the constant force of crystallization accelerates during the "reeling in" process.[1] Though other definitions of n have

on occasion been used for illustration, that appropriate to the near-ideal reptation model as derived in eqs 24a, 24b, and 24c in ref 1 is $n = M_{nw}/M_{(-CH_2-)} = (M_n M_w)^{1/2}/M_{(-CH_2-)}$ where $M_{(-CH_2-)} = 14$.

In the expression for i and other expressions to follow the activation energy for reptational transport is treated using the Arhennius form $\exp(-Q_D^*/RT)$ rather than the Vogel or "WLF" form $\exp[-U^*/R(T - T_\infty)]$. The latter holds up to crystallization temperatures of about $T_g + 100$ °C where T_g is the glass transition temperature. All of the PE growth rate data treated here, including those in regime III, refer to temperatures well above $T_g + 100$ °C where the Arhennius form applies.

Regime I appears at low ΔT where the nucleation rate is low *provided* there exists a substrate of finite length L. In such a situation a single primary nucleation act can lead to completion of the substrate of length $L = n_L a_0$ where n_L is the number of stems and a_0 is the width of a stem, thus completing a layer of thickness b_0 prior to the occurrence of another primary event (mononucleation). As will be brought out later, there is good evidence that L in PE is associated with the inherently small {110} growth fronts typical of lenticular crystals.

The growth rate in regime I is defined as

$$G_I \equiv b_0 i L = b_0 i n_L a_0 \tag{2a}$$

which on substituting for i (eq 1) leads to the growth rate in cm s^{-1} for regime I

$$G_I = G_{0(I)} \exp\left(\frac{-Q_D^*}{kT}\right) \exp\left(\frac{-K_{g(I)}}{T\Delta T}\right) \tag{2b}$$

where the preexponential factor is

$$G_{0(I)} = \frac{C_I}{^2/_3 n} = C_0 n_L \left(\frac{\kappa}{^2/_3 n}\right)\left(\frac{b_0 kT}{h}\right)\left(\frac{kT a_0(\Delta h_f)(\Delta T)}{4 b_0 l_u \sigma^2 T_m}\right) \tag{2c}$$

and the nucleation exponent

$$K_{g(I)} = \frac{[4] b_0 \sigma \sigma_e T_m}{(\Delta h_f) k} \tag{2d}$$

Values of C_I above and C_{II} and C_{III} to follow that are based on experimental data in the $M_{nw} = 30$K class are tabulated in ref 1 and are useful in estimating $G_{0(I)}$, $G_{0(II)}$, and $G_{0(III)}$ in lower molecular weight range $B-B'$where near-ideal reptation is followed. The left-hand equality in eq 2c gives the relationship which is subsequently employed to find $G_{0(I)}$ from the tabulated C_I value for this class. Similar relationships hold for $G_{0(II)}$ and $G_{0(III)}$ for MW range $B-B'$.

The nucleation rate i increases very rapidly with increasing ΔT because of the kinetically dominant factor $\exp(-4 b_0 \sigma \sigma_e T_m/(\Delta h_f)(\Delta T) kT)$ so that at a temperature T_{I-II}, multiple primary surface nucleation acts will begin to take place on a {110} substrate. In this situation regime II is entered where the growth rate is defined as

$$G_{II} \equiv b_0 (2ig)^{1/2} \tag{3a}$$

where g is the substrate completion rate in centimeters/second in one direction (right or left) from the initiating primary nucleus. This leads to

$$G_{II} = G_{(0)II} \exp\left(\frac{-Q_D^*}{kT}\right) \exp\left(\frac{-K_{g(II)}}{T\Delta T}\right) \tag{3b}$$

where

$$G_{(0)II} = \frac{C_{II}}{(^2/_3)\, n} = C_0^{1/2} \left(\frac{\kappa}{^2/_3 n}\right)\left(\frac{b_0 kT}{h}\right)\left(\frac{a_0(\Delta h_f)(\Delta T)}{\sigma T_m}\right)\left(\frac{kT}{2 b_0 \sigma l_u}\right)^{1/2} \exp\left(\frac{-q}{2kT}\right) \tag{3c}$$

and

$$K_{G(II)} = \frac{[2] b_0 \sigma \sigma_e T_m}{(\Delta h_f) k} \tag{3d}$$

In the above, q is the work of chain folding $2 a_0 b_0 \sigma_e$. It is important to observe that the substrate completion rate g in eq 3a, which has the form

$$g = a_0 \left(\frac{\kappa}{^2/_3 n}\right)\left(\frac{kT}{h}\right)\left(\frac{a_0(\Delta h_f)(\Delta T)}{\sigma T_m}\right) \exp\left(\frac{-Q_D^*}{kT}\right) \exp\left(\frac{-q}{kT}\right) \tag{4}$$

is much less dependent on ΔT than i, with the result that G_{II} varies as $i^{1/2}$. The expression for g is valid in regimes I and II, but the concept of "substrate completion" in the sense of eq 4 is largely replaced by the rapid deposition of the closely spaced primary stems in regime III (see below). Note also that g, like the surface nucleation rate i (eq 1) contains the terms of the transport factor β.

In regime II, the formula for the mean number of stem widths between primary (first stem) nucleation events is

$$S_k/a_0 \equiv (1/a_0)(2g/i)^{1/2} = \left(\frac{8 b_0 l_u \sigma}{kT}\right)^{1/2} \left(\frac{1}{C_0^{1/2}}\right) \exp\left(\frac{-q}{2kT}\right) \exp\left(\frac{+K_{g(II)}}{T(\Delta T)}\right) \tag{5}$$

At the junction with regime III, i.e., at T_{II-III}, ΔT_{II-III}, the value of S_k/a_0 should be ~1.5−2.0, i.e., a center-to-center distance of ~$1.5a_0$ to ~$2.0a_0$ between primary stems. The lower bound of $n_{III} \cong 1.5$ is initially set by the insightful solid-on-solid simulation of "three regime" behavior given by Guttman and DiMarzio.[7] Thus, at T_{II-III} and below the closely spaced primary stems characteristic of regime III appear as a result of the highly temperature-dependent surface nucleation rate.

The minimum value of n_{III} of ~1.5 noted above originated in the "stems only" simulation of Guttman and DiMarzio, and the question arises of how this concerts with the situation in a more or less chain-folded system. The question is considered in approximate terms in the appendix. The model is based on the trajectory of a given molecule with both sharp adjacent re-entrant folds as well as "loose" folds as it attaches to the substrate. The model pictures how n_{III} can be as low as ~1.5 in a nominally chain-folded system, and relates n_{III} to the degree of strictly adjacent re-entry and the mean sharply chain-folded cluster size in regime III.

At the higher temperature junction with regime I, i.e., at T_{I-II}, ΔT_{I-II}, the value of S_k/a_0 should approximate n_L, the number of stems of width a_0 comprising the

regime I substrate length L. In previous work it was estimated that S_k/a_0 was about 190 at ΔT_{I-II} and here we shall employ this value as well as 125 in calculating ΔT_{I-II}. Given the required constants, eq 5 can be used to calculate the temperatures and undercoolings of the I−II and II−III regime transitions and will be so employed in the case of both $M_{nw} \cong 30$K and $M_{nw} = 70.3$K. Equation 5 is expected to lead to acceptable results for both fractions for ΔT_{I-II} and ΔT_{II-III} since in the ratio g/i the factor κ should cancel whether the reptation be near-ideal or perturbed. This prediction will be subjected to experiment.

The parameter κ in eqs 1 and 4 is inversely proportional to the monomeric friction coefficient ξ_0 associated with reptation in the normal melt, and has the value of 0.77 where reptation is relatively unperturbed as in $M_{nw} \cong 30$K. For the time-average force f_c in the relation $g \propto f_c/n\xi$, κ is given by $h \exp(Q_D^*/RT_0)/\xi_0\, \delta l_{fold}$ where T_0 is a fixed reference temperature in the normal melt (449 K), ξ_0 is the monomeric friction coefficient at T_0, $\delta = kT/b_0\sigma$, and l_{fold} is the length of a fold.[1] [Input data for κ for near-ideal reptation: $\xi_0 = 7 \times 10^{-10}$ (erg s cm^{-2} = dyn s cm^{-1}) at $T_0 = 449$K, $Q_D^* = 5736$ cal mol^{-1}, $\delta = 10^{-7}$cm, and $l_{fold} = 6 \times 1.273 \times 10^{-8}$cm, which yields $\kappa = 0.77$.[1]] If reptation is perturbed, as in 70.3K, the effective monomeric coefficient increases, thus reducing κ below 0.77 and thereby lowering the growth rate. It is emphasized that a fall of κ below 0.77 is caused by the perturbation, and not the normal increase of $\xi(T)$ with lowering temperature already accounted for by the factor $\exp(-Q_D^*/RT)$ in eqs 2b, 3b, and 6b. Accordingly determination of κ affords a direct measure of the extent of the perturbation effect and will be so employed in the analysis of 70.3K. Note further that it is the independent determination of κ for near ideal reptation (together with the experimental value of C_0) which sets the stage for the quantitative evaluation of i and g based on eqs 1 and 4 for both $M_{nw} \cong 30$K and 70.3K that is featured later in this work.

The growth rate in regime III, where ΔT and therefore i is large, is defined as

$$G_{III} \equiv b_0 i n_{III} a_0 \tag{6a}$$

Using eq 1 this yields

$$G_{III} = G_{0(III)} \exp\left(\frac{-Q_D^*}{RT}\right) \exp\left(\frac{-K_{g(III)}}{T(\Delta T)}\right) \tag{6b}$$

with

$$G_{0(III)} = \frac{C_{III}}{^2/_3 n} = C_0 n_{III} \left(\frac{\kappa}{^2/_3 n}\right) \left(\frac{b_0 kT}{h}\right) \left(\frac{kT a_0 (\Delta h_f)(\Delta T)}{4 b_0 l_u \sigma^2 T_m}\right) \tag{6c}$$

and

$$K_{g(III)} \cong \frac{[4] b_0 \sigma \sigma_e T_m}{(\Delta h_f) k} \tag{6d}$$

The approximate notation of eq 6d is employed because the fold surface in regime III is taken to be less ordered than in regimes I and II. We also note that it has been predicted that regime III involves deposition in two lattice planes,[7] but here we retain the traditional version involving deposition on only one lattice plane.

Comparison of the nucleation exponents in eqs 2d, 3d, and 6d show that the relationship between them comes to

$$K_{g(III)} \cong K_{g(I)} = 2K_{g(II)} \tag{7}$$

This key prediction is a direct reflection of the nucleation regime aspects of the treatment wherein $G_I \propto i$, $G_{II} \propto i^{1/2}$, and $G_{III} \propto i$ as given by eqs 2a, 3a, and 6a, which in turn is the fundamental basis of the three regimes in PE. (Recall that in the case of $G_{II} = b_0(2ig^{1/2}$ the ΔT dependence of g is nil compared to that of the dominant factor i.) The validity of eq 7 will be examined, especially with regard to regime III, employing the present results on fraction $M_{nw} = 70.3$K as well as results from earlier studies at $M_{nw} \cong 30$K. This test will be dealt with first in the discussion of results since the other tests noted hinge on the $K_{g(i)}$ values obeying eq 7 with reasonable precision.

Following up on the effects of reptation, observe from eqs 2, 3, and 6 that within a given regime one has to a good approximation

$$G_{\Delta T(\text{constant})} \propto \frac{1}{n} \tag{8}$$

Holding ΔT constant ensures that the mean force of crystallization does not vary with n, and also mutes the variation of $\exp(-K_g/T(\Delta T))$. This places the variation of G with n in the preexponential factor as in the development. Equation 8 holds at least approximately for PE fractions in regime II in the molecular weight range $M_{nw} = 15.3$K to 38.6 K (range $B-B'$ of ref 1, near-ideal reptation), but exhibits a fall off in G well beyond $1/n$ in the range $C-C'$, $M_{nw} = 53.6$K to 90.6K, clearly indicative of perturbed reptation. Accordingly, perturbed reptation effects are anticipated in the present work on $M_{nw} = 70.3$K.

The same basic flux-based treatment leading to growth rates in the three regimes described above also gives the mean value of the *initial* lamellar thickness l_g^* prior to subsequent isothermal thickening. The expression is

$$l_g^* = \frac{2\sigma_e T_m}{(\Delta h_f)(\Delta T)} + C_2 \tag{9}$$

in which the constant C_2 in the "low ψ" form of nucleation theory consists of $\delta \cong kT/b_0\sigma$, a term involving the small temperature dependence of σ_e, and the thickness d_a of any amorphous surface zone.[1] (In an advanced form that considers fluctuations of the fold period and justifies the existence of a constant mean value of l_g^* at fixed ΔT for long substrate runs[8] in regimes I and II in the absence of the secondary process of isothermal thickening, a fold surface roughness term may be added to C_2.) Of particular interest here is the fact that l_g^* for PE does not depend on the regime of crystallization. A plot of l_g^* for PE fractions $M_{nw} \sim 30$K rises smoothly with decreasing ΔT with no breaks at either T_{II-III} or T_{I-II} in accord with eq 9 and experiment (see Figure 14 of ref 1).

It remains to be noted that many of the parameters in the kinetic treatment outlined above for $G(T)$ can be measured or calculated independent of surface nucleation theory. This is clearly true of Δh_f and T_m, and σ_e and q can be found from thermodynamic measurements

as well as from molecular energy calculations—for the latter see ref 9 as an example. Meanwhile the friction coefficient ξ_0 and thence κ have been derived from diffusion data with the help of reptation theory, as noted previously, and Q_D^* is directly determined from diffusion studies. There also exist useful empirical relations as well as an independent theory[1,10,11] for σ that holds for PE which is consistent with the "low ψ" formulation of nucleation theory—the theory for σ features an intermediate "segmentalized" and "aligned" surface state that resembles a physically adsorbed α-"rotator" phase.[1] Further, simulation provides an estimate of n_{III}.[7] The configurational path degeneracy C_0 that enters the treatment through eq 1 and acts as a scaling parameter can only be obtained from growth rate experiments, but this constant is well-behaved and has a single fixed value appearing directly as C_0 in the preexponential for regimes I and III and as $C_0^{1/2}$ for regime II. The above background provides useful input data and a helpful redundancy for a number of key quantities.

Experimental Section

The linear polyethylene fraction employed was of M_{nw} = 70.3K and polydispersity 1.12. To obtain sufficiently accurate spherulite growth rate results for this fraction over the range of ΔT required to exhibit the three regimes necessitated the use of special sample preparation and apparatus. These involved the following: (a) removal by hot filtration in solution of any excessive number of heterogeneous motes that initiated spherulites so that those remaining led to spherulites that grew to a size prior to impingement that were suitable for growth rates studies; (b) the formation of very thin solvent-cast films and other steps to facilitate dissipation of the heat of fusion, especially at the large undercoolings of regime III; (c) full removal of solvent in the cast thin film; (d) development of an automated system capable of measuring and recording time, temperature, and actual spherulite images as they grew isothermally.

As in previous work,[2] a sufficient reduction in the number of motes was achieved by filtering a 0.1 wt % solution of the fraction in distilled and prefiltered *p*-xylene three times through a 0.2 μm pore diameter filter at 125 °C. The filtrate was cooled to 85 °C where crystallization occurred, and the precipitate was filtered at 85 °C and then washed with more hot *p*-xylene. This pretreatment did not perceptibly alter the molecular weight distribution as confirmed by size exclusion chromatography. *This is important because it showed that no significant fractionation occurred during the crystallization at 85 °C.* (We note that the narrow fractions in refs 1 and 2 were pretreated in a similar manner.) A thin film was then solvent cast from *p*-xylene on a clean coverslip, with embedded thermocouple, melted under nitrogen at 145 °C, and residual solvent removed under vacuum for 36 h at 100 °C. *(Trials had shown that residual solvent lowered the transition temperatures slightly and the K_g values significantly.)* Films made in the manner noted were free of residual solvent and were typically 13−17 μm thick as determined by profilometry. The ultrafine thermocouple wire was 12.7 μm in diameter. The PE film−glass coverslip−thermocouple assembly was covered with a second coverslip using a Kapton spacer and the whole sealed with epoxy under a nitrogen environment. The upper coverslip was very close to but did not contact the PE film. The nitrogen in the assembly discouraged oxidation of the fraction. The thermocouple in the PE film in the sealed assembly was calibrated at 5 °C intervals from 100 to 135 °C. In practice, the temperature in the PE sample was known to better than 0.1 °C with a precision of a few hundredths of a degree.

Isothermal crystallizations were carried out using a Linkam TH600 hot stage in which the sealed sample assembly was situated on a temperature-controlled metal block heater with a sapphire window. The hot stage was purged with nitrogen and modified to accommodate the thermocouple leads. A silicone rubber O-ring was used to restrict nitrogen flow between the sample assembly top coverslip and the hot stage upper window thus allowing the sample top coverslip to warm to near the crystallization temperature.

A Zeiss polarizing optical microscope equipped with a video camera and a time-lapse VCR was employed, and a computer used to control the VCR and correlate and record time, temperature, and video data. The sample was situated such that the embedded thermocouple was just outside the field of view. A run was usually begun by heating the sample to a temperature T_1 = 154 °C, which is above T_m, for 1 min and then cooling to the desired crystallization temperature. For certain high crystallization temperatures in regime I, the spherulites were sometimes nucleated at lower temperatures (after first being taken to T_1) and then warmed rapidly to the desired T; this resulted in a better defined growth front but did not affect the growth rates. For certain low crystallization temperatures the rate of cooling to T was improved by increasing the flow of cold nitrogen through the heating block during cooling from T_1. Spherulites could be grown to about 150 μm diameters before impingement. At all temperatures the growth was lineal in time up to the point of impingement. The PE specimen was surrounded by glass or nitrogen and never heated above 154 °C in an effort to prevent oxidation. Regime II and III crystallizations took from under a minute to several hours. Regime I runs took from hours to days. Regime I runs were carried out last. As a check for oxidation a shorter run, near T_{II-III}, was repeated after each long run in regime I. Data collection was terminated if sample oxidation was noted as observed by the onset of nonlineal growth in regime I and a subsequent slower than expected growth rate in the repeated shorter run. The data reported here for M_{nw} = 70.3K refer to a full master run that exhibited all three regimes and which never exhibited oxidation effects.

For a given specimen the same set of spherulites, usually three in number, was used for nearly all runs. Spherulite initiation was usually of the heterogeneous type born at t = 0. Exceptions resulted from additional spherulite initiation in lower regime III and some delayed initiation in upper regime I, both being commonly observed effects. For regimes II and III the radial growth rates, G, for the measured spherulites of a given run were generally within 10%. Repeat runs at the same temperature were also within 10% as averaged for the set of three spherulites. In regime I, there was a somewhat larger error in G (15−30%), partly because the spherulite images were less circular and more poorly defined and partly because of the increased temperature variation during the much longer runs. Nevertheless the regime I data were still sufficiently accurate to establish a credible $K_{g(I)}$ value.

Self-heating effects as exhibited by a slowing of the growth rate during a run at low temperatures were not observed. Instead the lowest temperature at which G could be measured in regime III was actually governed by the rapidity with which the sample could be cooled from T_1 down to a settled isothermal crystallization temperature without meanwhile during the temperature equilibration process having the spherulites reach a state of impingement on each other. At the lowest temperature in regime III where it was practical to obtain isothermal measurements for M_{nw} = 70.3K, namely T = 116.50 °C, the growth rate was 4.9×10^{-4} cm/s while at the highest temperature in regime I, T = 130.71 °C, the growth rate was 5.4×10^{-9} cm/s. Thus, in a temperature range of 14.2 °C, crystal growth occurred in three regimes and the growth rate changed by almost 5 orders of magnitude.

Figure 2 shows representative examples of data for the increase of spherulite radius with time for three isothermal growth temperatures for each regime. The growth rate G was taken as the average of the least squares slopes of the radial growth vs time data for all monitored spherulites. All G vs T data for 70.3K, a total of 41 points, were based on similar plots. The adjacent optical micrographs in Figure 2 show the spherulite types present in each regime at the crystallization temperature corresponding to the middle set of points (middle crystallization temperature) for each regime. A discussion of

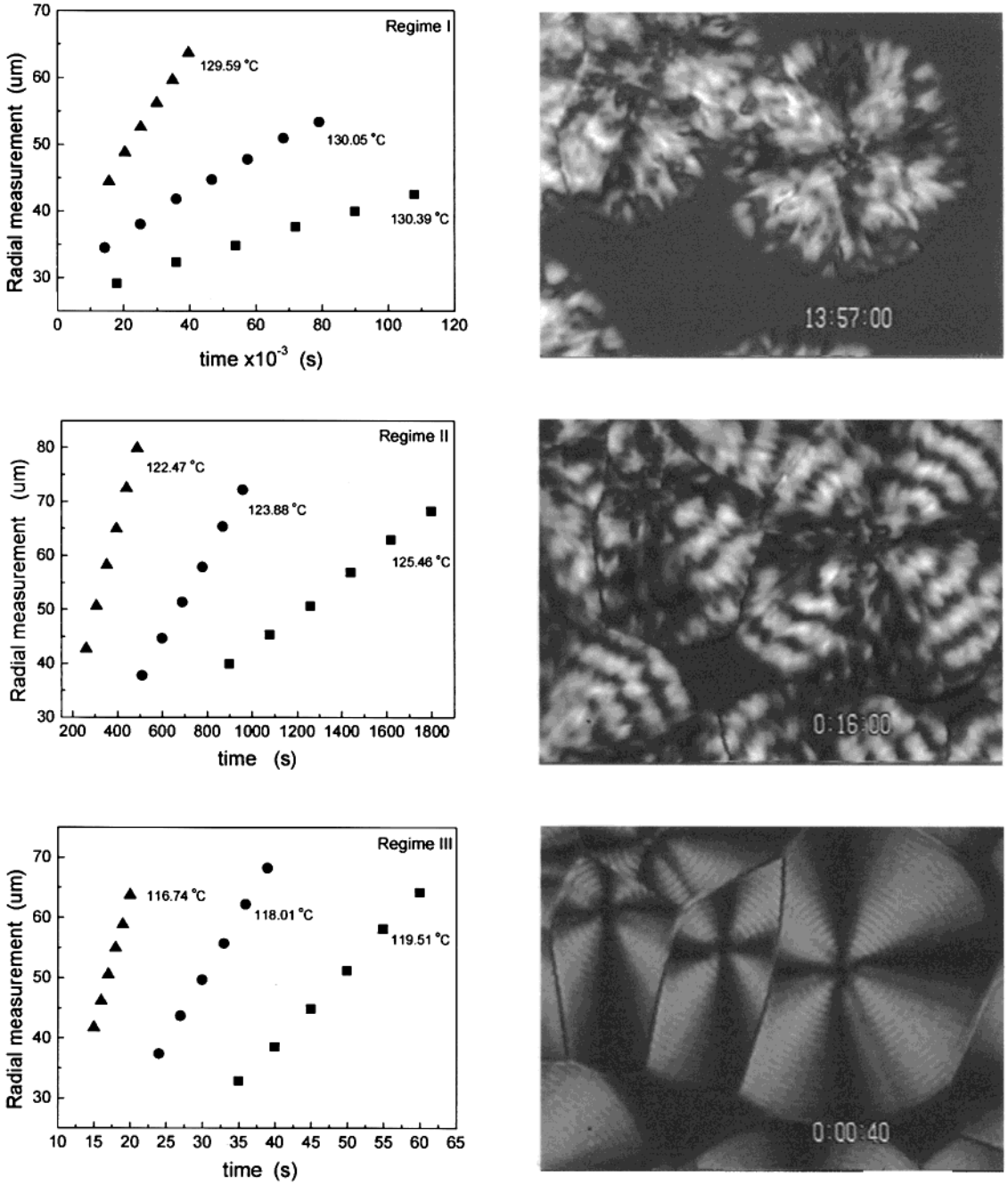

Figure 2. Spherulite radial growth vs crystallization time plots for fraction 70.3K for three crystallization temperatures in regimes I, II, and III. Radial measurements for each spherulite were taken from a discrete feature near the center and measured outward to the growth front and thus do not necessarily extrapolate to zero growth at zero time. On the right are optical micrographs of spherulites grown at the middle of the three temperatures in the adjacent plot. The height of the inset time characters corresponds to about 8 μm.

the variation of the band spacing with crystallization temperature is given in section G of the Results and Discussion.

Results and Discussion

A. Test of Relationships between K_g Values and Related Topics. A test of the relationships set forth in eq 7 between the K_g's for the various regimes is now considered which will include a comparison of the nucleation constants found in earlier work with new results for $M_{nw} = 70.3$K. The values of the melting point and Q_D^* required for the analysis of $M_{nw} = 70.3$K are given in Table 1a. Figure 3 depicts a plot of ln $G + Q_D^*/RT$ against $1/T(\Delta T)$ for the growth rate data for $M_{nw} = 70.3$K based on eqs 2b, 3b, and 6b. It is evident that all three regimes are present, the plot resembling in form the theoretical prediction shown in Figure 1 for a $M_{nw} \cong 30$K fraction. For a given regime, the slope of the straight-line portion in such a plot yields K_g for that regime and the intercept yields the corresponding preexponential G_0. There is slight curvature (heretofore not observed experimentally for a narrow PE fraction) close to both the I−II and II−III transitions. These small departures from "straight-line" behavior in the immediate vicinity of the regime transitions were avoided in determining the K_g values.[15]

The K_g and G_0 values for $M_{nw} = 70.3$K for each regime are listed in Table 1b. For reference, it is noted that from each of the K_g values it is determined that the

Table 1. K_g and G_0 Values for the 70.3K PE Fraction from ln $G + Q_D^*/RT$ vs a $1/T(\Delta T)$ Plot with Comparison with Theory and Earlier Work and Consideration of Near-Ideal and Perturbed Reptation

a. Input Data

param	value	source
T_m, melting point	144.7 °C for 70.3K 143.6 °C for 30K	Flory and Vrij[12]
Q_D^*, activation energy for reptational diffusion	5736 cal mol^{-1}	Fletcher and Klein[13]

b. Results for K_g

param	av for 10 fractions (M_{nw} sets $B-B'$ and $C-C'$, ref 1) and M_{nw} = 15.3K to 90.6K	present results for M_{nw} = 70.3K (deg^2)	temp range for M_{nw} = 70.3K[b] (°C)
$K_{g(I)}$	1.91×10^5	1.98×10^5	regime I, >128.9
$K_{g(II)}$	0.955×10^5	0.940×10^5	regime II, 120.9−128.9
$K_{g(III)}$	$\sim 1.91 \times 10^5$ [a]	1.85×10^5	regime III, <120.9
$K_{g(I)}/K_{g(II)}$	2.0	2.11	
$K_{g(III)}/K_{g(II)}$	~ 2.0[a]	1.97	

c. Values for $G_{0(j)}$ for $M_{nw} \cong 30$K (Near Ideal Reptation) and M_{nw} = 70.3K (Perturbed Reptation)

param	$M_{nw} \cong$ 30K, member of 7 fractions of set B−B′, ref 1, 15.3K to 38.6K	M_w = 70.3K, this work, member of 3 fractions of set C−C′, ref 1, 53.6K to 90.6K	
$G_{0(I)}$	$\sim 1.6 \times 10^{10}$ cm s^{-1}	$\sim 1.4 \times 10^{10}$ cm s^{-1}	
$G_{0(II)}$	5.45×10^3 cm s^{-1}	1.02×10^3 cm s^{-1}	*2.33×10^3* [d]
$G_{0(III)}$	1.75×10^8 cm s^{-1}	1.65×10^7 cm s^{-1}	*7.47×10^7* [d]
χ_c at T_{I-II}	~ 0.80[e]	~ 0.65[e]	

[a] Expected value based on theory that $K_{g(III)} \cong K_{g(I)} = 2K_{g(II)}$; $K_{g(I)}$ and $K_{g(II)}$ represent observed averages for all 10 fractions. This $K_{g(III)}$ is consistent with growth rates found at 90 °C and 100 °C for a fraction M_w = 32.1K (NBS SRM 1483) by Barham and Barham et al.[3] as shown in Table 3 of ref 1 and the T_{II-III} observed by Fatou et al.[4] from bulk crystallization measurements as shown in Figure 1 of this work. [b] Ranges based on intersection of $G(T)$ for adjoining regimes with straight-line approximation (solid lines on Figure 3). [c] $G_{0(j)}$ values for $M_{nw} \cong$ 30K based on $C_j = C_I$, C_{II}, and C_{III} values listed in Table 3 of ref 1 calculated with $G_{0(j)} = 1.5C_j/n$ with n set at nominal value of 2000. [d] Near-ideal reptation values for G_0(70.3K) calculated by multiplying G_0(30K) by the factor 30/70.3 = 0.427. [e] χ_c is degree of crystallinity at end of stage 1 crystallization (roughly at the point of robust spherulite impingement) at128°C as estimated from data of Mandelkern et al.[14] See also Figure 7b of ref 1.

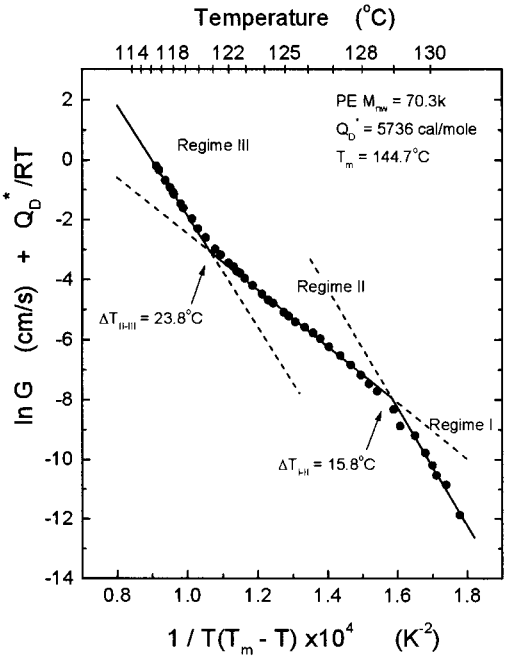

Figure 3. Plot of ln $G + Q_D^*/RT$ vs $1/T(\Delta T)$ showing the three crystallization regimes in a PE fraction M_{nw} = 70.3K, this work. Solid lines represent "straight line" fit of theory with G_0 and K_g values given in Table 1. Dashed lines show extrapolation of "straight line" fit regions; note slight deviations from linear behavior in the immediate vicinity of ΔT_{I-II} and ΔT_{II-III}.

product $\sigma\sigma_e$ is close to 1060 erg^{2}cm^{-4}, the components being nominally $\sigma_e \cong 90$ erg cm^{-2} and $\sigma \cong 11.8$ erg cm^{-2}. The principal contribution to σ_e is taken to arise from the mean work of chain folding q as averaged over the predominant population of "tight" folds according to $\sigma_e = q/2A_0$, where A_0 is the cross-sectional area of the PE chain. The reference states for σ_e and σ are the random coil melt (initial state) and the orthorhombic crystal (final state).[1]

It is seen in Table 1b that the K_g's for M_{nw} = 70.3K are close to the averages reported previously for regimes I and II, and it is significant that the K_g for regime III for M_{nw} = 70.3K is close to that assumed on the basis that $K_{g(III)} \cong K_{g(I)}$ employed in constructing Figure 1 for $M_{nw} \cong$ 30K. In no case does the difference between the K_g's for $M_{nw} \cong$ 30K and M_{nw} = 70.3K for a given regime exceed 3.7%. It is evident that eq 7 is obeyed quite well. The conformity of the K_g values to eq 7 implies that the average σ_e and σ values in the three regimes are close to the same. Also shown are the important K_g ratios for 70.3K, which hold within reasonable limits to expectation. This means that the fundamental concepts that $G_I \propto i$, $G_{II} \propto i^{1/2}$, and $G_{III} \propto i$ in eqs 2a, 3a, and 6a basically reflect correct physics, with the special note that the undercooling dependence of g in eq 3a ($G_{II} = b_0(2ig)^{1/2}$) must, as proposed, be negligible compared to that of i in the same expression to allow the agreement found experimentally.

It is concluded that the regime concept as stated in eq 7 is essentially correct for narrow fractions of linear PE in the range M_{nw} = 15.3K to 90.6K for regimes I and II as found in previous work and reinforced by the present study on 70.3K. Further, with regime III now being known to occur not only for M_{nw} = 30.5K but also for M_{nw} = 70.3K, the case for occurrence of growth in this regime at high ΔT in narrow fractions M_{nw} = 15.3K to 90.6K is strengthened. It is evident from Table 1b

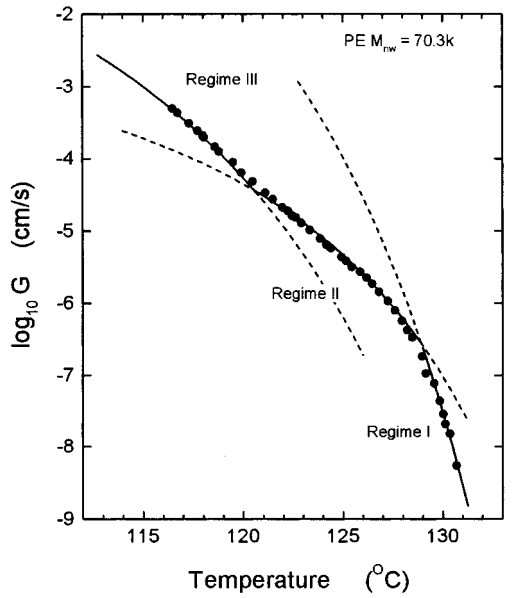

Figure 4. Observed growth rate data for PE fraction M_{nw} = 70.3K plotted vs crystallization temperature. Solid lines for $G(T)$ calculated with the same Q_D^*, G_0, and $K_{g(i)}$ values employed in Figure 3; dashed lines are extrapolated regime lines from $G(T)$ calculations. Actual data require use of three $G(T)$ curves to obtain good fit showing existence of three regimes. Note small deviations in transition regions as in Figure 3.

that the nucleation constants K_g hold their values within a given regime essentially independent of whether the transport process is near-ideal reptation (set $B-B'$) or perturbed reptation (set $C-C'$). The distinction between near-ideal and perturbed reptation will appear in the preexponential factors G_0.

For purposes of clarification, certain points relating to the existence of regimes need to be considered. While in the case of PE fractions the analysis of data is not critically dependent on the value of Q_D^* which is in any case accurately known, the analysis to obtain K_g does depend importantly on the value of T_m which decides the undercooling ΔT. The reader will observe that we have employed the Flory−Vrij equation[12] to estimate T_m, the extrapolated melting point for a fraction assuming an equilibrium content of paired chain ends. So far as a test of eq 7 is concerned, we could have employed the similarly based Broadhurst[16] extrapolation, also with an appropriate $R \ln n$ entropic term, that yields a T_m about 0.7 °C lower for M_{nw} = 70.3K. When analyzed with the Broadhurst T_m of 144.0 °C, the growth rate data for 70.3K lead to $K_{g(I)} = 1.81 \times 10^5$, $K_{g(II)} = 0.88 \times 10^5$, and $K_{g(III)} = 1.76 \times 10^5$ deg^2. The K_g ratios come to $K_{g(I)}/K_{g(II)} = 2.06$, $K_{g(III)}/K_{g(II)} = 2.00$, and $K_{g(I)}/K_{g(III)} = 1.03$ which are in good agreement with eq 7—note similarity to ratios in Table 1b based on T_m of 144.7 °C.

It is instructive to examine the appearance of a plot of growth rate data in the form of log G vs T, which removes the influence of the melting point and the degree of undercooling from the data presentation. Figure 4 shows such a plot for M_{nw} = 70.3K, the solid circles representing the observed data. The solid lines representing G for a specified regime were calculated with the K_g for that regime listed in Table 1b together with the corresponding G_0 given in Table 1c; eqs 2b, 3b, and 6b were employed to calculate $G(T)$ for regime I, II, and III, respectively. Thus, the curved solid lines in Figure 4 relate directly to the solid straight lines in Figure 3, the latter representing the "straight line" fit that ignores the slight curvature close to the transition regions. It is emphasized that the fit of the data points in the main body of each regime (i.e., that part of a regime away from the short transition zone) in Figure 4 is excellent, but could not have been so without the existence of all three regimes. Figure 3 exhibits the regime effects most clearly showing the slope changes of close to 2.0 in accord with eq 7 while Figure 4 gives a useful direct visualization of the nature of the untreated data that directly supports the existence of three separable states (regimes) of growth rate behavior without introduction of a melting point and the degree of undercooling. Figure 4 in particular shows that the "three regime" effect actually exists in 70.3K irrespective of other considerations.

It is useful to consider the question of the deviations from "straight line" behavior in the plot in Figure 3 of $\ln G + Q_D^*/RT$ vs $1/T(\Delta T)$ exhibited by the narrow molecular weight fraction 70.3K in the immediate vicinity of the I−II and II−III transitions. The extent of the deviation can be seen in Figure 3 where the solid lines (and extrapolated dashed lines) represent what we have termed "straight line" behavior. Such an effect was predicted by Frank in 1974 on a mean field basis[17] for the case of the I−II transition and by others with similar results utilizing different approaches.[18−20] By employing Frank's nucleation-based treatment as related to the Lauritzen Z_L plot for a PE fraction it was calculated that the maximum deviation of growth rate data from the straight line extrapolations at the I−II transition is a factor of 1.326 in G; further it was found that the deviation fell to a factor of 1.10 in G at 0.9 °C above the transition in regime I and at 1.14 °C below T_{I-II} in regime II (ref 1, p 3178). Though the natural scatter of the data points in regime I near the I−II transition in 70.3K prevents a precise comparison with theory, it is evident that the deviation is in the predicted direction and in at least general accord with the theory for the deviation. Experimentally the maximum deviation at the II−III transition is better defined, comes to a factor of $\sim 1.23 \pm 0.12$ in G in the opposite direction, and also diminishes quite rapidly on either side of the transition.

It is fitting at this stage to remark on the posit by Point[21] that what we have termed "regime transitions" in moderate molecular weight PE are really a result of fractionation effects during crystallization; were this correct it would undermine the regime concept which provides some of the best support for the viability of surface nucleation theory for PE in the molecular weight range just mentioned. In ref 21, Point does show some segregation effects (change of molecular weight distribution after crystallization) in low molecular weight 1.5K to 6.0K PEO fractions where the "breaks" in the growth rate data, rather than reflecting regime transitions, are commonly understood to be the result of the sequence: extended-chain → once-folding → twice folding and so on with increasing ΔT, i.e., "quantized" chain folding. (A nucleation-based treatment gives the undercoolings at which these "quantized" transformations in low M PEO take place.[22]) However in ref 21 these "breaks" in the low M PEO fractions, actually a result of quantization effects, are confused with the changes of slope of the type depicted in Figures 1 and 3 of the present work that represent true regime transitions,

and which appear only at moderate M and not low M. No evidence was given in ref 21 for the presence of segregation effects in PEO in the relevant moderate M range. In the case of PE the "breaks" in the growth rate data in the low M range 3.4K to ~10K resulting from "quantized" chain folding are easily distinguished from the regime transitions seen in the moderate M range 15.3K to 90.6K, and each have been described and quantitatively treated[1]. Further, as noted in the Experimental Section, crystallization of the 70.3K narrow PE fraction from dilute solution followed by washing with excess solvent at the crystallization temperature led to no perceptible change in the molecular weight distribution which remained at a polydispersity of 1.12. This discourages the idea that the regime transitions exhibited by 70.3K as in Figure 3 are caused by segregation effects. To this we would add that no explanation has been tendered for how segregation alone could cause three "regime-like" effects with slope changes of 2.0 between them such as shown in Figures 1 and 3. In sum, the concept that regime transitions are caused primarily by segregation in narrow PE fractions appears to be unsupported both experimentally and theoretically, and we shall proceed on the basis that surface nucleation theory with regimes included is applicable in the range of molecular weight of 15.3K to 90.6K emphasized in the present study.

B. Near-Ideal and Perturbed Reptation. The data given in Table 1b are clear on the issue that regime concepts as embodied in eq 7 are basically intact for the entirety of regimes I and II from 15.3K to 90.6K. This includes the new results for 70.3K in these two regimes, which closely match earlier measurements.[2] The new results for 70.3K for regime III also fit the regime picture given in eq 7, and are in general consistent with the existence of this regime for PE with $M_{nw} \cong 30$K (Figure 1).

With this background, we examine the question of "near-ideal" reptation, which is present between 15.3K and 38.6K, and "perturbed" reptation which occurs in the higher range 53.6K to 90.6K. A plot of log G vs log n at constant ΔT in regime II as prescribed by eq 8 showed approximate agreement with a $G \propto 1/n$ law for fractions 15.3K-38.6K, but exhibited deviations in the form of significantly lower growth rates for fractions in the higher range 53.6K to 90.6K (see figure 8 of ref 1, which includes $M_{nw} = 70.3$K). We note that the fractions that showed approximate agreement with the near-ideal reptation concept were in the group 15.3K to 38.6K and exhibited high crystallinity, while those in the higher range that showed marked deviation from the $G \propto 1/n$ law were of notably lower crystallinity (Table 1c). This will become important in the interpretation. In what follows, we shall bring regime III into the picture. The main issues are conveniently dealt with by considering a fraction in the vicinity of 30K (near-ideal reptation) and one of 70.3K (perturbed reptation). Before proceeding, it is well to note that a law based on a viscosity concept, namely $G_{(\Delta T \text{ constant})} \propto 1/n^{3.4}$, was never encountered even though the molecular weights were far above M_e. Accordingly, the resistance to transport of chains to the growth front is appropriately treated in terms of forced reptational diffusion, either near-ideal or perturbed, in the molecular weight range of interest here.

According to the theory, the behavior of the transport mechanism for each regime is contained in the preexponential factors as in eqs 2c, 3c, and 6c. Table 1c gives the preexponential factors $G_{0(i)}$ obtained for a fraction close to $M_{mw} \cong 30$K as deduced from C_I, C_{II}, and C_{III} values from previous work[1] as described in footnote (c) of Table 1. Because of the naturally occurring somewhat larger error in regime I measurements, the emphasis in what follows will be on regimes II and III. Also shown in Table 1c are the observed preexponential factors for $M_{nw} = 70.3$K, again with emphasis on regime II and III. In the case of $M_{nw} = 70.3$K, the numbers in normal type for $G_{0(II)}$ and $G_{0(III)}$ are the experimentally determined values. The numbers *in italics* in the fourth column of Table 1c were obtained by multiplying the results for $M_{nw} \cong 30$K by the factor 30/70.3 as based on the concept that the ideal G_0's for $M_{nw} = 70.3$K conform to $1/n$ behavior.

It is evident from the results in the last column of Table 1c that the preexponential factors for $M_{nw} = 70.3$K as actually measured experience a retardation that is significantly beyond that expected on the basis of $1/n$ behavior for the preexponential factors (fourth column of Table 1c). In the case of regime II, the additional retardation resulting from perturbed reptation is a factor of 2.3, and for regime III it comes to a factor of 4.5. While establishing the reality of the perturbation effect and its increase in going from regime II to regime III, these results are to be regarded as preliminary because there remains an effect on the perturbation values just cited because of small deviations (seen in Table 1b) of the K_g values from their ideal ratios as given by eq 7. It will subsequently be shown in a more detailed analysis based on the behavior of i and g for 70.3K that the perturbation effect increases regularly as one proceeds from regime I through III.

The central question here is the cause of the perturbed reptation effect in $M_{mw} = 70.3$K and its absence, or near absence, in $M_{mw} \cong 30$K. At this point we note the degree of crystallinity χ_c data in Table 1c for $M_{mw} \cong 30$K, which actually remains close to 0.80 for the entire set 15.3K to 38.6K, and note further that χ_c for $M_{nw} = 70.3$K is substantially lower at 0.65. (The degree of crystallinity given here refers to that present at the end of stage 1 crystallization at the crystallization temperature of 128 °C, and does not reflect any additional crystallization attained after cooling to room temperature; the temperature 128 °C is in general close to the I−II regime transition.) Beginning just above ~40K, PE fractions exhibit a decreasing χ_C with increasing M which falls to a value of 0.2−0.3 near 600−700K and then levels off at this low value (see Figure 7 of ref 1 and ref 14). The point here is that the perturbed reptation effect is definitely associated with a lowered degree of crystallinity, while near-ideal reptation is connected with a high and essentially constant χ_c. This suggests the following interpretation. The perturbation is the result of the longer dangling chain of the 70.3K fraction being drawn on to the substrate by the force of crystallization, forming some transient attachments elsewhere in the same (or another) lamella that impede the steady-state "reeling in" reptation process; some of these attachments become permanent (forming tie chains and loops) and lower the degree of crystallinity. Both the transient and permanent attachments are clearly fewer for the shorter chains 15.3K to 38.6K, thus muting the perturbation effect and at the same time allowing a high degree of crystallinity to develop.

In the molecular weight range 15.3K to 38.6K, κ is 0.77, and given the constant C_0 (see Table 2), the

Table 2. Calculation of ΔT_{II-III} and ΔT_{I-II} for $M_{nw} \cong 30$K (Near-Ideal Reptation) and $M_{nw} = 70.3$ (Perturbed Reptation) by the S_k/a_0 Method and Comparison with Experiment as well as Estimates of n_{III} and n_L

a. Input Data

param	value	source
a_0, width of stem, {110} face	4.55×10^{-8} cm	
b_0, thickness of stem, {110} face	4.15×10^{-8} cm	
l_u, C−C distance along chain axis	1.273×10^{-8} cm	
Δh_f, heat of fusion	2.8×10^9 erg cm^{-3}	
σ, lateral surface free energy	11.8 erg cm^{-2}	ref 1
q, work of chain folding	4.90 kcal/mol	ref 1, for $\sigma_e = 90$ erg cm^{-2}
C_0, configurational path degeneracy	4.41×10^5	ref 1, from regime I and II data
$K_{g(II)}$, regime II nucleation constant	0.955×10^5 deg^2	ref 1, from regime II data
	Trial Values	
$S_k/a_0 = n_{III}$ for ΔT_{II-III} calculation	$n_{III} = 1.5$ and 2.0	this work and ref 7; see footnote *a*
$S_k/a_0 = n_L$ for ΔT_{I-II} calculation	$n_L = 125$ and 190	

b. ΔT_{II-III} Calculated and Observed for $S_k/a_0 = n_{III} = 1.5$ and 2.0 (°C)

	$n_{III} = 2.0$	$n_{III} = 1.5$	obsd
ΔT_{II-III} for $M_{nw} \cong 30$K, ref 1	23.4	24.1	24.2 ± 0.3[b]
ΔT_{II-III} for $M_{nw} = 70.3$K	23.35	24.05	23.8[d]

c. ΔT_{I-II} calculated and observed for $S_k/a_0 = n_L = 125$ and 190 (°C)

	$n_L = 125$	$n_L = 190$	obsd
ΔT_{I-II} for $M_{nw} \cong 30$K, ref 1	16.5	16.0	16.4 ± 0.5[1]
ΔT_{I-II} for $M_{nw} = 70.3$K	16.4	16.0	15.8[c,d]

d. Estimate of L and $n_L = L/a_0$ by S_k/a_0 and Other Methods

method	value	remarks
(i) predicted extent of {110} substrate in regime I by S_k/a_0, his work	n_L about 120−200 L about 55−90 nm	see results in part c above for $M_{nw} \cong 30$K and $M_{nw} = 70.3$K; see also $i-g$ results, Table 3b
(ii) range of lattice coherence, D_{110} line widths (samples regime I crystallized)	39 nm, $n_L \sim 86$ (ref 24) 72 nm, $n_L \sim 158$ (ref 25)	based on suggestion by Frank[17] that L may be associated with the range of lattice coherence (see text)
(iii) electron microscopy	L in the range of several tens of nm upper bound $L \sim 100$ nm; $n_L \sim 220$	for pristine lenticular single crystal ({110} tip) $M \cong 14$K and M ≅ 32K (Toda[26]) estimated dimensions for growth tips or $M \cong 32$K pristine lenticular crystals from original micrographs supplied to authors by Toda (see refs 27 and 28 for earlier publication)

[a] The value $n_L = 190$ was originally determined from growth rate data in regimes I and II for samples in the range $B-B'$ (near-ideal reptation), and calculated from eq 30 of ref 1 using values of C_I, C_{II}, and κ in same source. [b] Estimated from Figure 3 of ref 4 (bulk crystallization rate data). Note also the use of this data point in Figure 1 of this work to mark the undercooling where regimes II and III intersect. [c] In the original study,[1] the value for this particular fraction, $M_{nw} = 70.3$K, was also slightly lower than that of other fractions and was determined to be $\Delta T_{I-II} = 15.9$ °C. [d] This work.

expressions for $G_{0(I)}$, $G_{0(II)}$, and $G_{0(III)}$ reproduce the observed preexponential factors generally within a factor of 1.1−1.3, which is satisfactory. (The other quantities such as Δh_f, q, and σ are independently known.) Thus, in this lower range, ξ and thence κ are not notably subject to perturbations of the reptation process that might be caused by the crystallization environment so that the theory for the preexponentials holds as expressed in eqs 2c, 3c, and 6c. The situation changes in the higher molecular weight range 53.6K to 90.6K, of which 70.3K is a member, because the effective friction coefficient increases owing to the perturbation that results from transient attachments during the "reeling in" process, thus leading to a reduced value of κ and thence a lower growth rate. For example, from the results for 70.3K in Table 1c, the predicted reduction in κ from 0.77 comes to $(1.02 \times 10^3/2.33 \times 10^3) \times 0.77$ giving $\kappa \cong 0.34$ for regime II, a result that will subsequently prove to be approximately correct. As implied earlier, the i and g analysis for 70.3K will provide more detail concerning the behavior of κ caused by the perturbation effect in this lower crystallinity fraction.

Later it will be brought out that both the reptation and regime picture in PE fractions change markedly above 100K, culminating at high M in low crystallinity with no distinct regime transitions with slope changes of ∼2.0 where the transport mechanism is increasingly reptation of "slack" , i.e., that process wherein only a small part of a dangling chain is drawn on to the growth front.[23] Slack also begins to be employed on a marginal basis in regime III in PE fractions of moderate M.[1]

C. Behavior of Absolute Values of i and g and Calculation of Growth Rates from Defining Relations in Each Regime for $M_{nw} \cong 30$K. It is of interest to consider the variation and magnitude of i and g as given by eqs 1 and 4. To verify the values of i and g, it will be shown that they serve to regenerate the growth rate data in the three regimes through the use of the defining relations as given by eqs 2a, 3a, and 6a. This will be carried out for the $M_{nw} \cong 30$K fraction using the nominal value $n = (M_n M_w)^{1/2}/M_{-CH_2-} = 2000$.

With the input data in Table 2a, eq 1 comes to

$$i \text{ (stems cm}^{-1}\text{ s}^{-1}) = 1.67 \times 10^{16}[T^2(\Delta T)] \times \exp\left(\frac{-2887}{T}\right) \exp\left(\frac{-1.91 \times 10^5}{T(\Delta T)}\right) \quad (10a)$$

The preexponential can be written with fair precision

because the factor κ is known to be 0.77 in the range $B-B'$ from evaluation of the monomeric friction coefficient as noted earlier. The quantity $2887/T$ is Q_D^*/RT where Q_D^* is known from diffusion studies and the 1.91×10^5 deg^2 corresponds to $4b_0\,\sigma\sigma_e T_m/(\Delta h_f)k$ where $\sigma\sigma_e = 11.8 \times 90 = 1062$ erg^2/cm.[4] The corresponding expression for the substrate completion rate as deduced from eq 4 for $n = 2000$ is

$$g\ (\text{cm s}^{-1}) = 1.42 \times 10^{-2}[T(\Delta T)] \times \exp\left(\frac{-5353}{T}\right) \quad (10b)$$

where the preexponential involves $\kappa = 0.77$ and other independently known quantities, and the exponent is $(q + Q_D^*)/RT$ where $q = 4900$ cal/mol and $Q_D^* = 5736$ cal/mol (Table 2a).

Using the above expressions, i and g are now calculated for the high and low undercooling extremes of regime II, namely $\Delta T_{II-III} = 24.2$ °C and $\Delta T_{I-II} = 16.4$ °C for $M_{nw} \cong 30$K (as in Figure 1). The results come to $i = 7.43 \times 10^{10}$ stems/(cm s) and $g = 1.62 \times 10^{-4}$ cm/s at $\Delta T_{II-III} = 24.2$ °C and $i = 7.58 \times 10^6$ stems/(cm s) and $g = 1.46 \times 10^{-4}$ cm/s at $\Delta T_{I-II} = 16.4$ °C. The variation of i is vastly greater than that of g in regime II; g increases by a factor of only 1.11 while i increases by a factor of 9800 with this nearly 8 °C change in undercooling. Accordingly our treatment wherein the growth rate G_{II} in regime II varies as $i^{1/2}$ with no significant variation being introduced by g is substantiated by direct calculation. While g does not appear in the defining relation $G_I = b_0 iL$ for regime I, it is easily rapid enough to cause completion of the substrate length L once a primary nucleus is injected thereon at the low rate i characteristic of this regime.

It can be shown that eqs 10a and10b can be employed together with the defining relations for G_i as expressed in eqs 2a, 3a, and 6a to calculate the actual growth rates for a specified regime for $M_{nw} \cong 30$K. We begin with the values for i and g cited above for the extremes of regime II at $\Delta T_{II-III} = 24.2$ °C and $\Delta T_{I-II} = 16.4$ °C. At $\Delta T_{II-III} = 24.2$ °C, $G_{II} = b_0(2ig)^{1/2}$ comes to 2.04×10^{-4} cm/s, and $G_{III} = b_0 i n_{III} a_0$ with $n_{III} = 1.5$ is 2.1×10^{-4} cm/s. Thus, the calculated growth rates match well at $\Delta T_{II-III} = 24.2$ °C at the junction between regimes II and III (Figure 1). Then with $G_{III} = b_0 i n_{III} a_0$ employed at 90 °C, $\Delta T = 53.6$ °C, where i from eq 10a comes to 2.3×10^{15} stems/(cm s), one finds with $n_{III} \sim 1.5$ that $G_{III} \cong 6.5$ cm/s, which is satisfactory since the observed value[1,3] of 3.5 cm/s holds to within a factor of 2−3. Thus, the regime III solid line in Figure 1 and its junction with regime II is reasonably predicted. At the junction of regimes I and II at $\Delta T_{I-II} = 16.4$ °C where $i = 7.58 \times 10^6$ stems/(cm s) and $g = 1.46 \times 10^{-4}$ cm/s, one finds with $G_{II} = b_0(2ig)^{1/2}$ that G_{II} is 1.95×10^{-6} cm/s and $G_I = b_0 i n_L a_0$ is 1.80×10^{-6} cm/s with $n_L = 125$ and 2.7×10^{-6} cm/s with $n_L = 190$. The experimental value of G at the I−II junction is $2.0 \pm 0.6 \times 10^{-6}$ cm/s, so the calculated results represent satisfactory agreement with experiment at this junction, where n_L comes to ∼140. The nucleation rate i is 9.86×10^3 stems/(cm s) at the lowest undercooling measured in regime I, $\Delta T = 13.3$ °C.[1,2] With $G_I = b_0 i n_L a_0$, this yields 2.3×10^{-9} cm/s with $n_L = 125$ and 3.5×10^{-9} cm/s with $n_L = 190$. The observed value is 3.2×10^{-9} cm/s, which implies a value of $n_L \sim 170$. Hence the regime I solid line in Figure 1 and its junction with regime II at $\Delta T_{I-II} = 16.4$ °C are well reproduced. Also, the regime II line is well predicted by the i and g values from eqs 10. The value of n_{III} employed above is from a solid-on-solid simulation,[7] and the values of n_L noted will be supported further in the S_k/a_0 treatment.

From the foregoing, it is concluded that eqs 10 for i and g with κ fixed at 0.77 are valid in that they reproduce the experimental growth rate results and the solid lines in Figure 1 representing the three regimes for $M_{nw} = 30$K with acceptable accuracy when combined with the defining relations as given by eqs 2a, 3a, and 6a, together with the values on n_{III} and n_L cited. The accuracy may be appreciated by observing that in going from $\Delta T = 13.3$ °C in regime I to $\Delta T = 53.6$ °C in regime III, i increased by a factor of over 10^{11}.

D. Analysis of *i* and *g* for M_{nw} = 70.3K and Determination of κ and Reduction Factor r. The ensuing treatment based on i and g for 70.3K serves to illustrate the perturbation of the reptational transport process in some detail by estimating κ in each regime. The treatment also provides insights concerning the behavior of the key parameters n_{III} and n_L for this fraction. The analysis consists of determining κ at points in each regime through applying appropriate expressions for i and g in the defining relations, eqs 2a, 3a, and 6a, such that the procedure reproduces the observed absolute growth rates. The value of κ will reflect the extent of the perturbation effect on reptational transport as it falls below the value 0.77, which is the norm for near-ideal reptation as in the higher crystallinity 30K fraction.

The relevant expressions for i and g with κ as the variable for the case where the prefactors in eqs 1 and 4 are based on $n = (M_n \times M_w)^{1/2}/M_{-CH_2-} = 5020$ as for 70.3K come to

$$i\ (\text{stems cm}^{-1}\text{s}^{-1}) = \kappa(8.63 \times 10^{15})[T^2(\Delta T)] \times \exp\left(\frac{-2887}{T}\right) \exp\left(\frac{-1.91 \times 10^5}{T(\Delta T)}\right) \quad (11a)$$

and

$$g\ (\text{cm s}^{-1}) = \kappa \cdot 7.32 \times 10^{-3}[T(\Delta T)]\exp\left(\frac{-5353}{T}\right) \quad (11b)$$

In these expressions, σ, σ_e, Δh_f, C_0, q, and Q_D^* are taken to hold their standard values as given in Tables 1 and 2. It is to be noted that the procedure is equivalent to setting $K_{g(III)} = K_{g(I)} = 2K_{g(II)} = 1.91 \times 10^5$ deg^2, which normalization cancels the small deviations between the standard K_g values and the experimentally observed values for 70.3K and noted in Table 1b, and in effect tends to smooth the results to be obtained for κ.

The growth rate data to be analzyed to obtain κ, n_{III}, and n_L for 70.3K were estimated from the "straight line" fits to the observed data using the K_g and G_0 values in Table 1b,c and eqs 2b, 3b, and 6b, and shown as the solid lines in Figure 3. Note that this fit ignores the small deviations of a factor of ∼1.2−1.3 in G that are confined to the immediate vicinity of the regime transitions. The analysis is carried out adhering to the concept that κ, i, and G are continuous at the regime transitions.

The analysis begins by establishing the value of κ for regime II employing eqs 11a and 11b for i and g in the defining relation eq 3a, $G_{II} = b_0(2ig)^{1/2}$, such that the growth rates are accurately reproduced as in Table 3a. At the junctions of regime I and II, the continuity

Table 3. Comparison of Theory and Experiment for M_{nw} = 70.3K: Calculation of G_I, G_{II}, and G_{III}, from *i*, *g*, and Defining Growth Rate Relationships for Each Regime and Estimation of κ, n_{III}, and n_L with Values of *i* Calculated from Eq 11a and *g* from Eq 11b

a. Regime II, $G_{II(calcd)} = b_0(2ig)^{1/2}$, Solving for κ Such That $G_{II(calcd)} = G_{II(obsd)}$

undercooling	$G_{II(obsd)}$ (cm/s)	*i* (stems/cm/s)	*g* (cm/s)	κ
$\Delta T_{I-II} = 15.8$ °C	$(2.9 \pm 0.3) \times 10^{-7}$	$i = 6.89 \times 10^5$	$g = 3.59 \times 10^{-5}$	0.467
$\Delta T = 20.0$ °C	$(5.34 \pm 0.53) \times 10^{-6}$	$i = 2.69 \times 10^8$	$g = 3.09 \times 10^{-5}$	0.369
$\Delta T_{II-III} = 23.8$ °C	$(3.0 \pm 0.3) \times 10^{-5}$	$i = 9.48 \times 10^9$	$g = 2.73 \times 10^{-5}$	0.315

b. Regime I, $G_{I(calcd)} = b_0 i n_L a_0$, Solving for n_L Using Extrapolated κ

undercooling	$G_{I(obsd)}$ (cm/s)	*i*	$\kappa_{(ext)}$[a] and n_L
$\Delta T = 14.0$ °C	$(5.4 \pm 1.0) \times 10^{-9}$	$i = 1.73 \times 10^4$ stems/(cm s)	$\kappa_{(ext)} = 0.52$; $n_L \cong 166$
$\Delta T_{I-II} = 15.8$ °C	$(2.9 \pm 0.3) \times 10^{-7}$	$i = 6.89 \times 10^5$ stems/(cm s)	$\kappa = 0.467$; $n_L \cong 224$

c. Regime III, $G_{III(calcd)} = b_0 i n_{III} a_0$, Solving for n_{III} Using Extrapolated κ

undercooling	$G_{III(obsd)}$ (cm/s)	*i*	$\kappa_{(ext)}$[a] and n_{III}
$\Delta T_{II-III} = 23.8$ °C	$(3.0 \pm 0.3) \times 10^{-5}$	$i = 9.48 \times 10^9$ stems/(cm s)	$\kappa = 0.315$; $n_{III} = 1.67$
$\Delta T = 28.2$ °C	$(4.9 \pm 0.5) \times 10^{-4}$	$i = 1.83 \times 10^{11}$ stems/(cm s)	$\kappa_{(ext)} = 0.27$; $n_{III} \cong 1.50$

[a] The expression $\kappa = 0.77/[0.0748 + 0.1\Delta T]$ fits the regime II results given in part a of this table (and other points not shown) to within 0.6% or better. This expression was used to estimate $\kappa_{(ext)}$ at $\Delta T = 14.0$ and 28.2 °C.

concept has κ and *i* already established by the regime II results which allows n_L to be found at ΔT_{I-II} with the defining relation $G_{I(calcd)} = b_0 i n_L a_0$ as in Table 3b. At the lowest undercooling in regime I, κ is estimated by a short extrapolation of the regime II results (see footnote of Table 3) to be close to 0.52. Then with *i* from eq 11a and this κ, the observed growth rate is reproduced with the defining relation for $G_{I(calcd)}$ yielding $n_L \cong 166$. A parallel procedure is carried out in Table 3c for regime III which leads with the relation $G_{III(calcd)} = b_0 i n_{III} a_0$ to a value of $n_{III} = 1.67$ at ΔT_{II-III} as well as the values of $\kappa_{(ext)} = 0.27$ and $n_{III} \cong 1.50$ at the highest undercooling for which data was obtained in this regime, $\Delta T = 28.2$ °C.

The values obtained for κ, n_{III}, and n_L for 70.3K are summarized in a plot of κ vs ΔT in Figure 5a. The value of κ is well below the near-ideal value of 0.77 throughout the experimental range falling from 0.52 at low undercooling, $\Delta T = 14$ °C, to 0.27 at $\Delta T = 28.2$ °C as regimes I, II, and III are traversed. These findings provide solid evidence for the presence of perturbed reptation in fraction 70.3K.

The average value of n_L in regime I is 195 ± 29 and leads to an *L* of ~90 ± 20 nm. The latter is taken to approximate the size of the {110} growth front active in regime I, and will be discussed more fully after the S_k/a_0 analysis is given. The values of n_{III} in regime III of ~1.5 at the largest ΔT in this regime and 1.67 at ΔT_{II-III} are consistent with the predictions of the modeling effort of Guttman and DiMarzio noted earlier. Generally similar values of n_L and n_{III} will be found for both $M_{nw} \cong 30$K and 70.3K in the S_k/a_0 analysis.

Observe in Table 3a that *g* in regime II varies by only a factor of 1.32 while *i* varies by a factor of 1.38×10^4. Thus, despite the presence of perturbation, the change in *i* still overwhelms that of *g* in regime II so that G_{II} indeed varies essentially as $i^{1/2}$ in 70.3K as required. The overall change in *i* for 70.3K increases by a factor of close to 10^7 as ΔT increases from 14 to 28.2 °C.

Consider now the independent evidence obtained previously for the perturbation effect in fraction 70.3K. In a plot of log G_{II} vs log *n* (ref 1 Figure 8b) for the constant undercooling of $\Delta T = 17.96$ °C in regime II, data for the molecular weight range $B-B'$ (samples ranging from $M_{nw} = 15.3$K to 38.6K) roughly follow the $G_{II\ constant\ \Delta T} \propto 1/n$ relation (eq 8 in present text) in agreement with near-ideal reptation as a transport

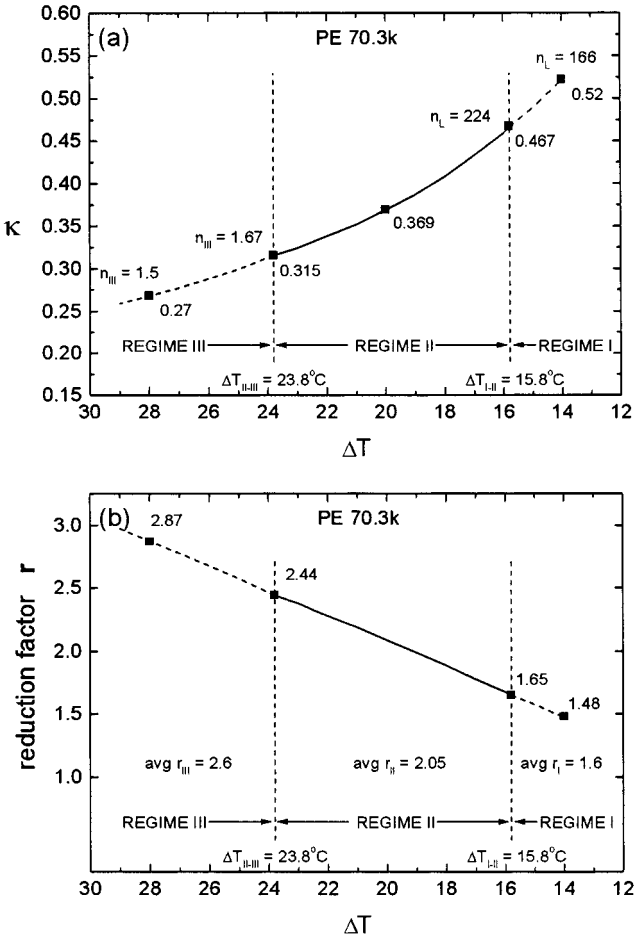

Figure 5. Reptational perturbation effect in fraction 70.3K (normalized K_g's): (a) Parameter κ as a function of ΔT, where numbers below the curved line give κ at various ΔT values and numbers above the line give n_{III} and n_L; (b) reduction factor **r** as a function of ΔT showing increased perturbation with increasing undercooling.

mechanism. Three higher molecular weight fractions in range $C-C'$ (M_{nw} = 53.6K, 70.3K, and 90.6K) fall significantly below the $1/n$ line indicating perturbed reptation. Fraction 9 in ref 1, Figure 8b, is the 70.3K fraction and shows a reduction in growth rate by a factor of ~2.5 below that expected for $1/n$ behavior. Below it will be shown that the κ values from the $i-g$ analysis

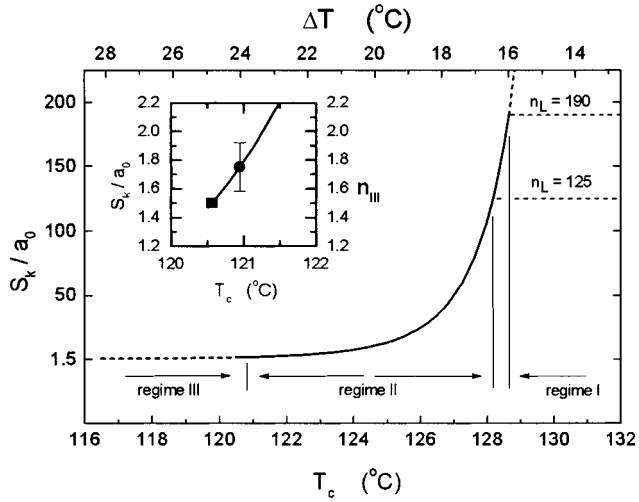

Figure 6. Plot of S_k/a_0 (number of stems of width a_0 between primary nucleation events in regime II) vs T and ΔT for PE fraction $M_{nw} = 70.3$K via eq 12, solid curve. Plot yields ΔT_{II-III} estimates for various n_{III} values and ΔT_{I-II} estimates for n_L of 125 and 190. Inset shows expanded view as S_k/a_0 approaches the theoretical lower bound of $n_{III} = 1.5$ at ■; data point (●) at 120.9 °C for $S_k/a_0 = 1.75 = n_{III}$ corresponds to interpolated observed central value of $\Delta T_{II-III} = 23.7$ °C in Table 2b. Rising curve for S_k/a_0 near $T = 128.7$ °C (ΔT_{I-II} of 16.0 °C) for n_L of 190 approximates the observed ΔT_{I-II} of 15.8−15.9 °C (Table 2c). Result for $S_k/a_0 = 125$ shown for comparison.

for this fraction yield approximately the same departure from $1/n$ behavior in regime II for 70.3K.

The dependence of the perturbation effect on undercooling for 70.3K is readily shown by plotting the degree of retardation as a function of ΔT. The degree of retardation r resulting from reptational perturbations is expressed as

$$r = 0.77/\kappa \qquad (11c)$$

When perturbation is absent, κ is 0.77 and r is unity. The value of κ cannot exceed 0.77, so r cannot have values below 1, but as r rises above unity, perturbatation is increasingly present.

A plot of r vs ΔT for 70.3K is depicted in Figure 5b. Observe that the average r_{II} is 2.05 in regime II, which is fair agreement with the factor of 2.5 obtained above from the $G_{II(\text{const }\Delta T)} \propto 1/n$ plot. Note that the reduction factor r rises in close to a linear manner from 1.48 at the lowest undercooling in regime I to 2.87 at the largest undercooling in regime III, showing an increase in the perturbation effect with increasing undercooling as was found for regimes II and III on a preliminary basis for 70.3K (Table 1c). The cause of the perturbation is the same as that stated earlier, but now with the firm insight that the labile chain attachments that hinder transport of the chain being drawn down to the growth front are more tightly bound by the larger driving potential[1] for crystallization, $\Delta G \propto \Delta T$, which is significantly stronger in regime III than in regime I. The finding that the perturbation effect is largest in regime III for 70.3K might allow a modest perturbation effect deep in this regime even for $M_{nw} \cong 30$K, but the growth rate data at $T = 90$ °C in Figure 1 for $M_{nw} = 30.5$K is of insufficient accuracy to confirm this.

E. Application of $S_k/a_0 = (1/a_0)(2g/i)^{1/2}$ to calculation of ΔT_{II-III} for $M_{nw} \cong 30$K and $M_{nw} = 70.3$K. Here eq 5 is applied to the problem of determining the undercooling ΔT_{II-III} for $M_{nw} \cong 30$K (near-ideal reptation) and $M_{nw} = 70.3$K (perturbed reptation). This provides a detailed test of the internal structure of the theory and specifically addresses the prediction that S_k/a_0 formulation should apply to both near-ideal reptation and perturbed reptation. Recall that this prediction arises from the circumstance that in the ratio $2g/i$ the factor κ that reflects the activity of the pertubation effect is present in both g and i and thus is absent through cancellation.

The required input data are given in Table 2a, all being standard values for PE based on previous studies.[1] With a_0, b_0, l_u, σ, q, $K_{g(II)}$, and C_0 inserted into eq 5, one has

$$S_k/a_0 \equiv (1/a_0)(2g/i)^{1/2} = 2.863\times 10^{-2} T^{-1/2} \times \exp\left(\frac{-1233}{T}\right) \exp\left(\frac{0.955 \times 10^5}{T(\Delta T)}\right) \qquad (12)$$

Calculation of ΔT_{II-III} is carried out with $(S_k/a_0) = n_{III}$ trial values of 1.5 and 2.0, the lower bound of 1.5 being based on the Guttman and DiMarzio "stems only" simulation[7] (see appendix for connection to a chain-folded system). In the calculations $T(\Delta T)$ for 30K was based on $T_m = 143.6$ °C and for 70.3K was based on $T_m = 144.7$ °C. A plot showing the behavior of S_k/a_0 as a function of T and ΔT for 70.3K is shown in Figure 6; the corresponding plot for 30K is similar and is not shown. The S_k/a_0 results in Table 2b show that the theoretical lower bound of $n_{III} = 1.5$ is closely approached in these cases, the observed values at ΔT_{II-III} corresponding to $n_{III} = 1.5$ for 30K and 1.75 for 70.3K. The $i-g$ analysis for 30K was consistent with $n_{III} \cong 1.5$ at ΔT_{II-III} and the $i-g$ analysis for 70.3K gave $n_{III} = 1.67$ at ΔT_{II-III}, which comprises good agreement with the S_k/a_0 method. Thus, at the lower temperature end of regime II where the II−III transition takes place, and where both regime II and regime III exhibit perturbed reptation in the 70.3K fraction but not in 30K, it is evident that eq 5 as expressed numerically by eq 12 applies with good accuracy irrespective of the presence or absence of perturbation in the reptational process as predicted on the basis of the cancellation of κ effect.

F. Application of the S_k/a_0 Formulation to Calculation of ΔT_{I-II} and Estimate of L and n_L: The Truncated Lozenge → Lenticular Crystal Transformation and the Origin of L in Regime I. It has been shown by Toda for PE fractions $M_w = 13.6$K, $M_n = 11.4$K, and $M_{nw} = 12.5$K[26] and for $M_w = 32.1$K, $M_n = 28.9$K, and $M_{nw} = 30.5k$[27] (both NBS−NIST SRM's) that the growth rate transition from regime I to regime II is associated with the change of crystal type as observed by electron microscopy for crystals extracted from the melt: truncated lozenge (regime II) → lenticular crystal (regime I). This is significant because it provided a new insight into the origin of the substrate length $L = n_L a_0$ for fractions noted above. The elongated lenticular crystal was taken by Toda on basic crystallographic grounds to have a very small {110} growth tip on which mononucleation takes place thus allowing growth in regime I in the b axis direction. The slower growing curved edges of the lenticular crystal were taken to involve of {200} folds. The less elongated truncated lozenge type of crystal formed at temperatures below the regime I−II transition has large {110} faces on which multiple nucleation can occur as is consistent with regime II growth. Based on Toda's work, one is justified in taking a truncated lozenge → lenticular

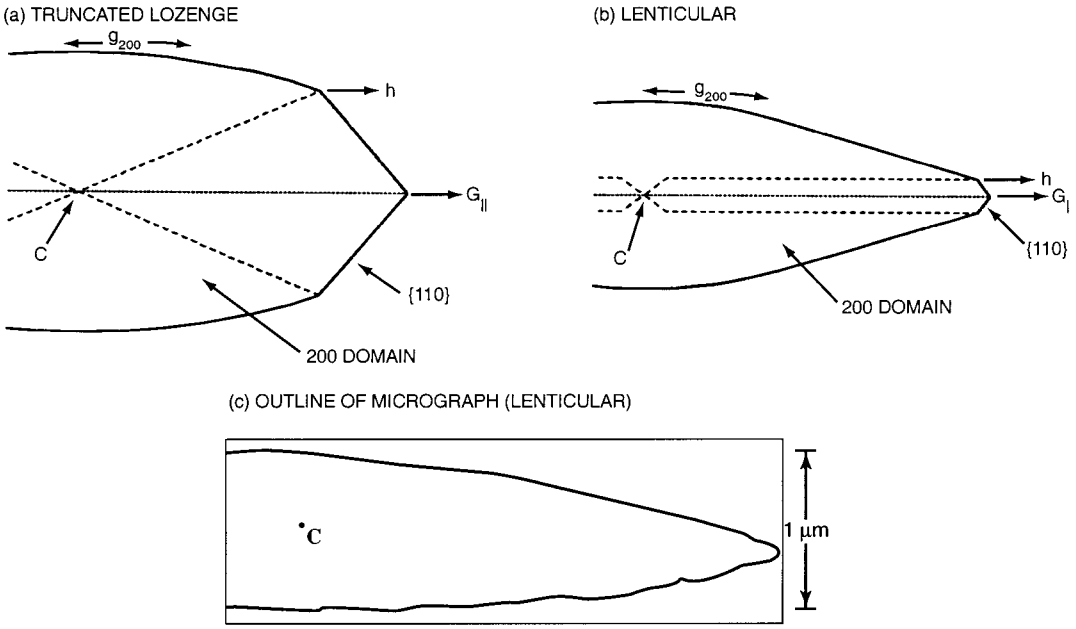

Figure 7. Crystal types in PE fractions in regimes I and II: (a) schematic of prototypical truncated lozenge, regime II, with large {110} growth front (Mansfield); (b) schematic of pristine lenticular crystal, regime I, with very small {110} growth front (Toda); (c) sketch of electron micrograph to scale for $M_{nw} \cong 30$K lenticular crystal extracted from the melt. "C" is the center of the crystal in all diagrams.

crystal transformation to be associated with $M_{nw} \cong 30$K fractions. Toda's study did not cover fractions in the vicinity of $M_{nw} = 70.3$K, but we shall initially assume that such a change of crystal type leading to a small {110} growth tip in regime I also occurs in this fraction, despite the fact that 70.3K did not exhibit strictly axialitic structures as observed by optical microscopy as did 30K in regime I.[1,2] (This point will be clarified in section G.) With this background concerning the nature of the {110} growth fronts in regimes I and II, we proceed to apply the S_k/a_0 formulation to the estimation of ΔT_{I-II} with eq 5 via eq 12 for $M_{nw} \cong 30$K and 70.3K for n_L trial values of 125 and 190.

Table 2c shows the ΔT_{I-II} calculated with eq 12 for the n_L values noted together with the observed ΔT_{I-II} values. For $M_{nw} \cong 30$K (near-ideal reptation) an n_L of slightly larger than 125 stem widths is closest to the central observed ΔT_{I-II} of 16.4 °C, but the error limit of ±0.5 °C is not exceeded for $n_L = 190$, the latter being the original estimate.[1] (Recall also that the $i-g$ analysis for 30K yielded $n_L \sim 170$ at $\Delta T = 13.3$ °C and $n_L \sim 140$ at ΔT_{I-II}.) For $M_{nw} = 70.3$K (perturbed reptation) the n_L corresponding to the observed ΔT_{I-II} is marginally greater than 190, but an n_L of 190 or somewhat less is allowed. It is significant that the result for n_L for 70.3K by the S_k/a_0 method of ∼190 is close to the average of that derived for regime I of (224 + 166)/2 or 195 by the $i-g$ approach (Figure 5a, Table 3b). The results for n_L for 30K and 70.3K imply that the "cancellation of κ effect" of the S_k/a_0 method is operative in each fraction as it was for n_{III}.

This work indicates that n_L for these fractions is indeed very small, falling in the range of about 120−200 stem widths on the {110} growth tip in regime I (Table 2d, item i). Further, the similarity of the results for n_L for 30K and 70.3K implies that our assumption that the 70.3K fraction involves a truncated lozenge → lenticular crystal transformation is tenable. After a more complete description of the crystal types involved in the I−II transition, we shall note independent estimates of n_L such as may be obtained from X-ray line-width studies and electron micrographs of pristine lenticular crystals.

The prototypical truncated lozenge (regime II) is a six-sectored crystal with four relatively large sectors with {110} growth fronts and two lateral sectors with {200} edges that are curved (sections of an ellipse) as described by the treatment of Mansfield[29,30] (Figure 7a). The long axis of the crystal corresponds to *b* axis growth and has large {110} growth fronts. The more elongated pristine lenticular crystal (regime I) has two large {200} sectors with curved edges, and importantly a very narrow {110} strip postulated by Toda to begin near the crystal center and extend along the *b* axis to the small {110} growth tips at either end[26,27] (Figure 7b). In Toda's treatment, it is these small {110} tips of the lenticular crystal that are the sites of the substrate length L on which mononucleation occurs thereby leading to regime I growth. Interestingly, the change in crystal type is governed by the relation $g_{200} < h$ for the lenticular crystal and $g_{200} > h$ for the truncated lozenge, where g_{200} is the substrate completion rate on the curved {200} edge and h the rate of advance of the {110} growth front parallel to the *b* axis (Figure 7a,b). The change of crystal type occurs when $h = g_{200}$. To induce the change of crystal type:truncated lozenge (regime II) → lenticular crystal (regime I), g_{200} must fall very rapidly with increasing T, which is in strong contrast with the minimal variation of g_{110} with T shown earlier in this work. The cause of the drastic fall in g_{200} has not been fully explained, though several schemes (e.g., "kinks" and "antikinks") have been suggested and discussed.[27] This does not alter the fact that the change of crystal type actually occurs, the lenticular crystal with its small {110} growth front providing the basis for regime I growth. The theory for the shape of the {200} sectors of the lenticular crystal does not specify the dimensions of the {110} growth tip.

With the above background, it is now possible to examine the question of the validity of the prediction by the S_k/a_0 method of the size of the {110} substrate in regime I. One approach to obtaining an independent

estimate of $L = n_L a_0$ that was employed in the past was based on the range of lattice coherence, D_{110}.[1] In the present context, D_{110} is assumed to be a measure of the width of the postulated narrow {110} strip in the lenticular crystal. The measured D_{110} values for PE crystallized in regime I would appear to support the S_k/a_0 estimates of L within a factor of about two (Table 2d, items i and ii), but the agreement is provisional because a detailed analysis is lacking. Estimation of the actual size of the {110} growth tip of a pristine lenticular crystal extracted from the quenched subcooled melt as seen in electron micrographs, presents a challenge because of its small size, but a value on the order of some tens of nanometers has been surmised by Toda (Table 2d, item iii). Our examination of the original electron micrographs of pristine lenticular crystals extracted from the melt for $M_{nw} \cong 30$K, kindly suppled to us by Prof. Toda, showed that the leading growth tips were somewhat damaged and the facets for the most part indistinct, but it was possible to estimate that the tips had an upper bound of about 100 nm (Table 2d, item iii). [We note also the presence of an asymmetric overgrowth[27,28] which appears to arise from the onset of a spiral terrace with a tip of ca. 150 nm for a $M_{nw} \cong$ 30K fraction, but it is not certain that the overgrowth formed in regime I rather than during the quench.] While clearly not exact, the independent estimates of L cited in Table 2d would appear to support the S_k/a_0 results for L at ΔT_{I-II} within a factor of about 2−3.

As matters now stand, we hold to our estimates of n_L within the stated limits partly on the grounds that the S_k/a_0 and $i-g$ methods are firmly anchored at ΔT_{II-III} by $n_{III} = 1.5-1.75$ by both modeling and experimental findings so one may anticipate reasonable results at ΔT_{I-II} as regards n_L by the S_k/a_0 and $i-g$ methods, and partly because the dimensions from electron microscopy for n_L are of the same general magnitude as that predicted by both methods (Table 2c,d).

The treatment given here for the I−II transition is consistent with the change of crystal morphology at the I−II transition revealed by Toda,[26,27] which leads to a natural explanation of the origin of the very small {110} growth fronts of the lenticular crystal system that defines the substrate length L in regime I. Attribution of L to the small lenticular system {110} growth front is clearly more satisfying than an arbitrary breaking up of a larger {110} front into smaller sections of the size L supposedly caused by "stopping defects" [1]—thus in both this and Toda's, work L is the *real* length of a small {110} tip (Figure 7b) and not a "persistence length" associated with dividing up a large {110} front.

It is emphasized that the change of crystal type at the I−II transition does not alter the basic proposition that mononucleation on a {110} substrate of length L is active in regime I and that regime II involves multiple nucleation on a {110} substrate—this concept has been held from the beginning and is inherent in the general expressions for growth in regimes I and II as expressed here and elsewhere.[1,2] Specifically, the expressions for G_I and G_{II} as given in the theory do not require modification because of the change of crystal type. However one now understands from the work of Toda that the small L leading to regime I growth is generated in the lenticular crystal system, and one sees further that the "multiple nucleation on a {110} substrate" characteristic of regime II refers to the larger {110} facets of the truncated lozenge crystal type.

No change of gross crystal type comparable to the striking lenticular crystal→ truncated lozenge transformation at the I−II regime transition is known to take place at the II−III transition, though a more subtle change of a different nature may occur, such as might derive from the predicted[7] development of stem deposition in more than one lattice plane in regime III. Accordingly, a detailed experimental study of this point would be of interest. As shown here by the S_k/a_0 method, the II−III rate transition is well represented from a kinetic point of view as a straightforward nucleation effect wherein the rate of injection of primary stems at rate i becomes so high relative to the rate of substrate completion g that with increasing ΔT in regime II these primary stems become very closely spaced and thereby become the predominant mode of surface addition (Figure 6). This leads to the shift from $G_{II} \propto i^{1/2}$ in regime II to $G_{III} \propto i$ in regime III. Viewed in this light, the II−III effect is the simpler of the two transitions.

G. Relationship between Spherulitic and Axialitic Structure and Regime Transitions. Here we note certain connections, or lack thereof, between spherulitic and axialitic structures as observed by optical microscopy on one hand and regime transitions as derived from growth rate studies on the other. It is well established for the range ∼15K to ∼40K, that the I−II transitions as observed by growth rate data correspond with a change from strictly axialitic structures in regime I to nonbanded spherulites in upper regime II as seen by optical microscopy.[1,2] Also in this range, the axialitic structures arise from lenticular crystals.[26,27] This situation applies to the $M_{nw} \cong$ 30K fraction; however, the 70.3K fraction, which has a definite I−II transition as shown in Figure 3, did not exhibit a strictly axialitic structure in regime I. In the early stages of growth the objects formed in regime I in 70.3K as observed by us using optical microscopy exhibited a distinct fibrous structure radiating from the center clearly indicative of an axialitic component, but when mature, the objects had evolved as nonbanded spherulites of somewhat irregular shape (noncircular growth boundary and irregular extinction characteristics) with none of the openness and spine-like appearance of the strictly axialitic structures observed in $M_{nw} \cong$ 30K and lower molecular weights. (Compare regime I optical micrograph for 70.3K in Figure 2 of the present work with Figure 6a of ref 1 which exhibits what we have termed a "strictly axialitic" structure for PE fraction $M_{nw} =$ 28k.) Considering the evidence for a fibrous element in 70.3K together with the fact that the S_k/a_0 analysis for 30K and 70.3K yielded similar results for n_L, it is apparent that the underlying basic crystal type in regime I for 70.3K is lenticular as is known to be the case for $M_{nw} =$ 30.5K.[26] It follows that regime I growth arising from lenticular entities is not always accompanied by the development of strictly axialitic structures when mature.

Both the 30K and 70.3K fractions undergo additional changes as seen by optical microscopy with further decreases in crystallization temperature below the I−II transition according to the scheme: nonbanded spherulites→ coarsely banded spherulites→ increasingly finely banded spherulites (Figure 2). This raises the question of whether the II−III transition as observed by crystallization kinetics is in some manner associated with the appearance of banding or a band spacing effect. For fractions of about 30K the onset of banding is close to

the II−III transition, but for 70.3K the banding begins about 4 °C above the II−III transition, i.e., about in the center of the 8 °C regime II window. Hence, the II−III transition is not in general associated with the onset of banding or a particular band spacing. Keith and Padden had previously noted the shift in the onset of banding to higher temperatures with increasing molecular weight for PE.[31]

H. Comparison of Broad and Narrow PE Samples with Similar M_{nw} Values. Wagner and Phillips (WP) have published spherulite growth rate measurements[32] for a whole polymer linear PE specimen $M_{nw} = 73.9$K, $M_w/M_n = 1.88$ over a wide range of temperatures, and it is of interest to briefly note certain similarities and differences with the present work on the narrow $M_{nw} = 70.3$K, $M_w/M_n = 1.12$ fraction. First, the WP whole polymer sample exhibited a II−III regime transition at 120.6−120.8 °C, and a value of 120.9 °C was found here for the narrow 70.3K fraction, which constitutes remarkable agreement. A significant difference appears, however, in the measured I−II regime transition. For the broad WP sample, T_{I-II} was 125.6 °C, whereas that of the narrow 70.3 fraction was $T_{I-II} = 128.9$ °C. The extent of regime II for the WP sample was thus only 4.8−5.0 °C, while that of the narrow 70.3K fraction was 8.0 °C (Figure 3). The latter is similar to the regime II range of 7.8 °C found for the narrow $M_{nw} \cong 30$K fraction (Figure 1). It is noted further that the slope changes at the regime transitions in the broad WP specimen are about 1.4 rather than being close to 2.0 as found for the narrow 70.3 fraction.

I. Cessation of Distinct Regime Transitions above $M = 100$K and Increasing Dominance of Reptation of "Slack" at High M: Regime III-A. In the immediate vicinity of $M_{nw} \cong 100$K, where the limiting crystallinity at the crystallization temperature as defined previously has fallen to $\chi_c \approx 0.50$, the regime I−II transition in PE fractions as observed by spherulite growth rates rather abruptly disappears as a distinct entity, the growth rates in the entire ΔT range where it formerly appeared then being represented by a single "mixed" K_g of $\sim 1.5 \times 10^5$ deg^2. With increasing molecular weight, this K_g is maintained up to $M_{nw} \sim 640$K, a molecular weight above which distinct spherulitic objects no longer appear.[2] It is of interest that even in the range 100K to 640K the spherulitic growth process can still be described by the pair G_0, K_g. At the highest molecular weights in the range $(5-8) \times 10^6$, the χ_c for PE has fallen to $\sim 0.20-0.30$ and K_g rises to $1.8-1.9 \times 10^5$ deg^2 as estimated[1] from $\ln \tau^{-1}$ vs $1/T(\Delta T)$ plots based on bulk crystallization rates.[33] These values of K_g and χ_c at ultrahigh M represent the properties of what is termed "regime III-A." (The general situation regarding K_g and χ_c as a function of M_{nw} is illustrated in Figure 7 of ref 1.) Thus, the type of growth at ultrahigh molecular weight denoted as III-A is characterized by a typical regime III nucleation constant K_g and a low degree of crystallinity. The low crystallinity bespeaks the presence of a massive degree of amorphous material between the imperfect microlamellae, some of it consisting of tie chains between different lamallae with much of the remainder being associated with long loops between mostly distant (nonadjacent) stems in a same lamella, in each case the amorphous chains being multiply pinned to crystals. Such structures in the ultrahigh molecular weight fractions rule out anything approaching the "near-ideal" or the weakly "perturbed" form of steady-state forced reptation as the transport process shown here to be active at $M_{nw} \cong 30$K and $M_{nw} \cong 70.3$K where clear-cut I−II and II−III transitions occur. Instead, only short sections of chains, the equivalent of one or at most two stem lengths, can be drawn on to the substrate by the force of crystallization with the reptation of slack process,[1,23] which is the only viable transport mechanism in regime III-A. With reptation of slack in such a torpid ultrahigh molecular weight system being unable to sustain any substantial substrate completion process of the type treated in regime II, the natural result is regime III-like behavior dominated by the deposition of primary stems and the concomitant absence of other regimes and the transitions between them. The disappearance of discrete regime transitions with slope changes of 2.0 between them at ∼100K may be viewed as being caused by the onset of a stronger form of the relatively weak "perturbed" reptation effect already shown here to be present in the 70.3K fraction. This stronger form would involve a larger number of permanent attachments per chain which would reduce the crystallinity and also incur increased employment of reptation of slack as a transport mechanism with further increase of molecular weight.

Summary and Conclusions

The aim of this work was to test surface nucleation theory as it is impacted by regime and reptation concepts for narrow PE fractions in the moderate molecular weight range of 15−90K with emphasis on fractions in the range $M_{nw} \cong 30$K and 70.3K. Fraction 30K is typical of the high crystallinity group 15.3−38.6K that exhibits "near-ideal" reptation and 70.3K is typical of the lower crytallinity group 50.3K-90.6K that exhibited "perturbed" reptation. The new experimental study on 70.3K provided needed information, particularly accurate spherulitic growth rate data in regimes II and III. Neither the I−II nor the II−III transitions were completely abrupt. The regime transitions were not caused primarily by fractionation and the presence of all three regimes is readily apparent even in a plot of log G vs crystallization temperature (Figure 4).

The results for 70.3K were compared with the growth rate data from earlier studies on $M_{nw} \cong 30$K which, like 70.3K, exhibited all three regimes. The first test was based on the experimental nucleation constants $K_{g(i)}$ where i = I, II, or III representing the three regimes with slope changes of 2.0 between them as obtained from the observed growth rates, G_i. Both fractions obeyed the predicted relation $K_{g(III)} \cong K_{g(I)} = 2K_{g(II)}$ with accuracy sufficient to show that $G_I \propto i$, $G_{II} \propto i^{1/2}$, and $G_{III} \propto i$ where i is the surface nucleation rate. The next test involved the preexponential factors $G_{0(i)}$, which measure the effect on the absolute growth rate of reptational diffusion and perturbations thereof as the chain is drawn onto the crystal substrate by the force of crystallization. It was shown that such perturbation occurred in 70.3K. The perturbation effect was attributed to an increase in the effective monomeric friction coefficient (as reflected in the lower preexponential factor κ in the basic expressions for the surface nucleation rate i and substrate completion rate g) caused by labile chain attachments some distance from where the longer chain of 70.3K was being drawn on to the substrate. The perturbation effect correlated well with the reduced degree of crystallinity of the 70.3K

fraction. A detailed analysis of the behavior of κ for 70.3K was carried out in terms of the fundamental expressions for i and g as combined with the defining relations for each regime which yielded accurate estimates of κ by comparison of calculated and measured growth rates, thus quantifying the reduction in growth rate caused by the perturbation of reptational transport in each regime. This analysis also yielded values of n_{III} and n_L for 70.3K, n_{III} being the characteristic number of stems of width a_0 at and below the II−III transition and n_L being the number of stem widths associated with the {110} substrate length L in regime I. Expressions for i and g were also developed for $M_{nw} \cong 30$K, and it was demonstrated that the absolute growth rates in each regime could be reproduced therefrom using the defining relations together with independently supportable values of n_L and n_{III}. In these expressions, the variation of i was far greater than that of g in regime II for both 30K and 70.3K, thus meeting a requirement of regime and nucleation theory. The evaluation of the absolute values of i and g for 30K stemmed from the independent determination of of the friction coefficient ξ_0 and thence κ for use in eqs 1 and 4 for the case of near-ideal reptation as combined with the experimental value of C_0. Extension to the perturbation effect in 70.3K as reflected by a reduced κ was then straightforward.

Another test involved the function S_k/a_0 that defines the spacing between primary stems in regime II. The expression for S_k/a_0 was first applied to the calculation of ΔT_{II-III} (junction of regimes II and III) for both 30K (near-ideal reptation) and 70.3K (perturbed reptation). The results that corresponded to the experimental ΔT_{II-III} were in each case at or close to $n_{III} = 1.5$ stem widths. This was a satisfactory outcome especially in view of the facts that (a) a simulation by Guttman and DiMarzio gave a similar result for the lower bound of n_{III} and (b) the S_k/a_0 formulation, as predicted, was not appreciably affected by the presence or absence of perturbed reptation. The S_k/a_0 method was then applied to the calculation of ΔT_{I-II} (junction of regimes I and II) for 30K and 70.3K. The observed ΔT_{I-II} values were matched with substrate lengths of $L = n_L a_0$ in the range 55−90 nm, with $n_L = 120-200$ stem widths. Basically similar values of n_{III} and n_L were found for 70.3K with the $i-g$ analysis mentioned above. Thus, the S_k/a_0 and $i-g$ methods are mutally supportive. From the limited independent information currently available, e.g., that from electron micrographs, the predicted values of L and n_L appear to be reasonable. The cessation near 100K and above of typical regime transitions with slope change of ~2.0 is attributed to a progressive increase in the perturbation of the chain transport process; at ultrahigh molecular weight, this leads to a single regime denoted III-A characterized by reptation of slack, low crystallinity, and a low degree of tight folding.

It is concluded that surface nucleation theory, as developed to include regime and reptation effects, leads to a more complete picture based on stated molecular mechanisms for the three regimes of crystallization in relatively narrow melt-crystallized PE fractions of moderate molecular weight than was heretofore available. The distinctive observed growth rate data for this simplest of crystallizable polymers cannot be accommodated and understood for narrow fractions in this range without consideration of the existence of the three regimes. The theory is internally consistent, the values of key parameters such as C_0, n_{III}, and n_L remaining firm within reasonable limits in varied applications, such as the S_k/a_0 formulation as compared with calculation of $G(T)$ for a specified regime from the quantified expressions for i and g using the defining relations. In general, the treatment is in accord with the crystal morphology of PE. Specifically the treatment of the I−II rate transition is now more directly in line with Toda's proposition that the lenticular crystal provides the small {110} substrate of length L in regime I.

Last it is noted that the treatment outlined in this and earlier work, which features the force of crystallization acting to reel a chain through the subcooled melt in a curvilinear reptational mode onto the growth front during substrate completion, has found utility in the recent work of others.[34] These authors showed that freshly melted extended-chain PE on subsequent crystallization in regime II initially exhibited a definitely reduced degree of melt entanglement as evidenced by a marked increase in the spherulite growth rate, which in time reverted to its slower normal rate as the equilibrium concentration of entanglements was reestablished. This result is of significance to the concept of entanglements in the melt and is supportive of the reptational aspects of nucleation theory as applied here to polymer crystallization from the normal entangled subcooled melt.

Acknowledgment. J.P.A. gratefully acknowledges funding support from the Office of Naval Research. The authors thank Dr. C. M. Guttman of NIST for helpful comments on the Guttman−DiMarzio paper (ref 7) and for discussions on removing nucleating agents from PE fractions as well as GPC studies. The authors are also grateful for helpful comments by Prof. H. D. Keith, University of Connecticut (banding in spherulites), and Dr. F. Khoury of NIST (crystallography). J.D.H. wishes to especially thank Prof. A. Toda, Hiroshima University, for a most useful discussion concerning lenticular crystals and for copies of original electron micrographs of such crystals.

Appendix

Two simple illustrations when subsequently combined are helpful in understanding the origin and meaning of n_{III}, which describes the close spacing of primary stems for a more or less chain-folded system in regime III. Special considerations apply here such that the model has both sharp and "loose" folds, the "loose" fold type being consistent with the extremely high nucleation rate i in this regime, and the sharp fold type being important because of its role in maintaining the $\sigma\sigma_e$ in $K_{g(III)}$ at the same level as that in $K_{g(I)}$ as in eq 7. To describe the situation in the partially disordered fold surface, we consider the molecular trajectory of a given molecule in regime III as it attaches to the substrate for two cases:

Case i: A primary stem denoted **p** is the first put down on the substrate followed with a strictly adjacent second stem denoted **s** as for normal substrate completion, the intervening chain fold being sharp, i.e., of the p_{ar} type. Now a third contiguous stem is added after an amorphous transit that because of the high nucleation rate i in this regime leaves a "loose" fold pinned in place on the lamellar surface by this new stem. This third stem with its quasi-amorphous connection to the second stem is denoted **p*** and is taken to have the character of a primary stem. The resulting three stem sequence

p−**s**−**p*** thus has two primary stems separated by a center-to-center distance of $2a_0$, i.e., $n_{III} = 2.0$.

Case ii: A primary stem **p** is first put down, and the high value of *i* induces deposition of a second stem of the **p*** type. This **p**−**p*** structure with its quasi-amorphous surface component has a center-to-center separation of a_0, i.e., $n_{III} = 1.0$. A **p**−**p*** structure (or the corresponding **p***−**p***) with its quasi-amorphous surface component is not counted as an adjacent re-entrant sharp fold, but rather as an "accidental" adjacency of two primary stems.

After an initial nucleation act **p**, a concatenated assembly of a mixture of cases i and ii for a long molecular trajectory in regime III may be schematically represented as

...−**p***−**s**−**p***−**p***−**s**−**p***−**p***−**s**−**p***−**p***−**s**−**p***−... →

In this molecular trajectory the nature of the traverse from a preceding stem to the next contiguous stem decides the character, i.e., **p*** or **s**, of the next stem added in sequence reading from left to right. If a stem already in place generates a random coil excursion before the chain puts down the next contiguous stem, that new stem is a "primary" **p*** stem; these are the structures **s**−**p*** and ***p****−**p***, each with an intervening "loose" fold. If on the other hand the emergent chain from a stem already in place immediately folds sharply with no amorphous transit and puts down a contiguous stem, that next stem is substrate completion **s**, leading to the structure **p***−**s** with an intervening sharp fold. In the limit of a long trajectory for the sequence above, the mean distance between primary stems **p*** is $1.5a_0$; i.e., $n_{III} = 1.5$, matching the lower bound of ∼1.5 of the "stems only" simulation of Guttman and DiMarzio.[7]

For a long trajectory, one-third of the folds on each lamellar surface are strictly sharp adjacent re-entrant, and two-thirds are quasi-amorphous "loose" folds. The quasi-amorphous surface component implies a reduced χ_c in regime III. Moreover, with the degree of strictly adjacent re-entry p_{ar} (fraction of sharp folds) being $^1/_3$ and given the alternative relation[1] $p_{ar} \equiv 1 - 1/\bar{\nu}_c$ where $\bar{\nu}_c$ is the mean sharply chain-folded cluster size, it is seen that this cluster size is 1.5 stems—this is another way of describing and understanding the lower bound of n_{III} in regime III.

Insertion of a slightly higher fraction of case i structures with spacing $2a_0$ between primary stems increases n_{III} above 1.5 and p_{ar} above $^1/_3$. Thus, for 70.3K where n_{III} is 1.5 at $\Delta T = 28.2$ °C and goes to 1.67 at $\Delta T_{II-III} = 23.8$ °C (Figure 5a), p_{ar} rises from 0.33 to 0.40, in good agreement with previous estimates for regime III.[1] It is evident from the adherence of growth rate data for 70.3K to eq 7 that the $\sigma\sigma_e$ in $K_{g(III)}$ is normal in regime III even though the fraction of sharp folds is only 0.33−0.40; this implies that the substrate completion process is largely regulated by the *q* of the sharp folds though "loose" folds likely also contribute.

While providing a schematic basis for the origin of the small n_{III} in a somewhat disordered chain-folded regime III, the model could be made more realistic by introducing some cilia that subsequently formed amorphous tie chains to other lamella in place of some of the loose folds. While not detailed here, the model can be extended to the body of regime II where p_{ar} increases further and where each surface patch in this regime can be described in the **p**, **s**, (and if needed) **p*** notation.

References and Notes

(1) Hoffman, J. D.; Miller, R. L. *Polymer* **1997**, *38*, 3151.
(2) Hoffman, J. D.; Frolen, L. J.; Ross, G. S.; Lauritzen, J. I., Jr. *J. Res. Natl. Bur. Stand., Sect. A* **1975**, *79*, 671.
(3) Barham, P. J. Private communication, 1982. Martinez-Salazar, J.; Barham, P. J.; Keller, A. *J. Polym. Sci. Phys. Ed.* **1984**, *22*, 1085.
(4) Fatou, J. G.; Marco, C.; Mandelkern, L. *Polymer* **1990**, *31*, 1685.
(5) Guttman, C. M.; DiMarzio, E. A.; Hoffman, J. D. *Polymer* **1981**, *22*, 1466.
(6) Mansfield, M. L. *Macromolecules* **1983**, *16*, 914.
(7) Guttman, C. M.; DiMarzio, E. A. *J. Appl. Phys.* **1983**, *54*, 5541.
(8) Lauritzen, J. I., Jr.; Passaglia, E. *J. Res. Natl. Bur. Stand., Sect. A* **1967**, *71A*, 261.
(9) Chum, S. P.; Knight, G. W.; Ruiz, J. M.; Phillips, P. J. *Macromolecules* **1994**, *27*, 656.
(10) Hoffman, J. D. *Polymer* **1992**, *33*, 2643.
(11) Hoffman, J. D.; Miller, R. L.; Marand, H.; Roitman, D. B. *Macromolecules* **1992**, 25, 2221.
(12) Flory, P. J.; Vrij, A. *J. Am. Chem. Soc.* **1963**, *85*, 3548.
(13) Fletcher, D. P.; Klein, J. *Polym. Commun.* **1985**, *26*, 2.
(14) Mandelkern, L.; McLaughlin, K. W.; Alamo, R. G. *Macromolecules* **1992**, *25*, 1440.
(15) The temperature ranges employed for determining the K_g's for M_{nw}=70.3k were 129.4−130.71 °C for regime I, 122.5−128.0 °C for regime II, and 116.5−119.0 °C for regime III.
(16) Broadhurst, M. G. *J. Res. Natl. Bur. Stand., Sect. A* **1966** *70A*, 481.
(17) Frank, F. C. *J. Cryst. Growth* **1974**, *22*, 233.
(18) Lauritzen, J. I., Jr. *J. Appl. Phys.* **1973**, *44*, 4353.
(19) Goldenfeld, N. *J. Phys. A* **1984**, *17*, 2807.
(20) Toda, A.; Tanzawa, Y. *J. Cryst. Growth* **1986**, *76*, 462.
(21) Point, J. J. *Macromolecules* **1997**, *30*, 1375; see page 1383.
(22) Hoffman, J. D. *Macromolecules* **1986**, *19*, 1124.
(23) Klein, J.; Ball, R. *Faraday Discuss. Chem. Soc.* **1979**, *68*, 198.
(24) Baltá Calleja, F. J.; Martinez-Salazar, J.; Čačkovič, J.; Laboda-Čačkovič, H. *J. Mater. Sci.* **1981**, *16*, 739.
(25) Vogel, W.; Haase, J.; Hosemann, R. *Z. Naturforsch.* **1974**, *29A*, 1152.
(26) Toda, A. *Colloid Polym. Sci.* **1992**, *270*, 667.
(27) Toda, A. *Faraday Discuss.* **1993**, *95*, 129.
(28) Toda, A.; Keller, A. *Colloid Polym. Sci.* **1993**, *271*, 328.
(29) Mansfield, M. L. *Polymer* **1988**, *29*, 1755.
(30) Mansfield, M. L. *Polym. Commun.* **1990**, *31*, 283.
(31) Keith, H. D.; Padden, F. J. *Macromolecules* **1996**, *29*, 7776.
(32) Wagner, J.; Phillips, P. J. *Polymer* **2001**, *42*, 8999.
(33) Ergoz, F.; Fatou, J. G.; Mandelkern, L. *Macromolecules* **1972**, *5*, 147.
(34) Psarski, M.; Piorkowska, E.; Galeski, A. *Macromolecules* **2000**, *33*, 916.

MA010313U